Crafting the multiferroic BiFeO3-CoFe2O4 nanocomposite for next-generation devices: A review

Journal:	*Materials and Manufacturing Processes*
Manuscript ID	LMMP-2021-0596.R1
Manuscript Type:	Review
Date Submitted by the Author:	23-May-2021
Complete List of Authors:	Amrillah, Tahta; Universitas Airlangga, Nanotechnology, School of Advanced Technology and Multidiscipline; Universitas Airlangga Hermawan, Angga; IMRAM Wulandari, Chandrawati ; Airlangga University, Faculty of Advanced Technology and Multidiscipline Muthi'ah, Aisyah ; Airlangga University, Faculty of Advanced Technology and Multidiscipline Simanjuntak, Firman; National Chiao Tung University, Department of Materials Science and Engineering
Keywords:	multiferroic, thin-film, nanocomposites, magnetoelectric, sensors, energy harvesting, photocatalytic, electrocatalysis, photovoltiacs, epitaxy

Crafting the multiferroic $BiFeO_3$-$CoFe_2O_4$ nanocomposite for next-generation devices: A review

Tahta Amrillah[a,*], Angga Hermawan[b], Chandrawati Putri Wulandari[a], Aisyah Dewi Muthi'ah[a], Firman Mangasa Simanjuntak[c]

[a]*Faculty of Advanced Technology and Multidiscipline, Universitas Airlangga, Surabaya 60115, Indonesia;* [b]*Institute of Multidisciplinary Research for Advanced Material (IMRAM), Tohoku University, 2-1-1 Katahira, Aoba-ku, Sendai, Miyagi, Japan 980-8577;* [c]*Department of Materials Science and Engineering, National Chiao Tung University, Hsinchu 30010, Taiwan*

Corresponding Author E-mail: tahta.amrillah@stmm.unair.ac.id

Crafting the multiferroic $BiFeO_3$-$CoFe_2O_4$ nanocomposite for next-generation devices: A review

$BiFeO_3$-$CoFe_2O_4$ (BFO-CFO) vertically aligned nanocomposite (VAN) thin-film promises great potentials for next-generation electronic devices. Its strong magnetoelectric, antiferromagnetic-ferrimagnetic, and structural couplings occur *via* large interface area interactions across the vertical surface between BFO and CFO phases; this leads to emergent exotic fundamental physics rendering its potential applications for various electronics such as magnetic sensor, data storages or memory devices, and energy harvesting devices. The distinctive photoactivity of both BFO and CFO phases in the BFO-CFO VAN system also can generate advanced applications as photovoltaic and photocatalytic devices. Furthermore, owing to small overpotential and excellent stability in alkaline media, BFO-CFO nanocomposites becomes the next electrode in electrocatalysis devices. The BFO-CFO VAN also have been exponentially developed having various type of thin-film architectures grown on various substrates. In this present article, we review the current status of the BFO-CFO VAN thin-film and discuss the fundamental understanding as well as the technology involved in developing this material. We also address the challenges that hinder the commercialization of this material and propose some plausible solutions to encourage BFO-CFO VAN-based electronic devices to reach their maturity level. Furthermore, the potential marketability of the BFO-CFO VAN materials and devices for future consumer products is also discussed.

Keywords: multiferroic; magnetoelectric, structural coupling; thin-film; nanocomposite; next-generation devices; sensors; data storages; energy harvesting device; photovoltaic; photocatalytic; electrocatalysis

Introductions

Multiferroic material possesses multiple characteristics of ferroic properties that attracted extensive research interest and developments for many applications.[1, 2] Various types of multiferroics were discovered depending upon its magnetic-electric interaction mechanisms; lone-pair-active multiferroics, geometric ferroelectricity, charge ordering, magnetically-driven ferroelectricity, *f*-electron magnetism, and

multiferroic composites. Particularly for multiferroic composites, this material possesses large magnetoelectric properties compares to other types of multiferroic. In general, a multiferroic nanocomposite is a combination of two materials having strong magnetic and electric properties that lead to strong magnetoelectric coupling.[3] A large number of material combinations have been discovered having unique magnetoelectric couplings mechanisms such as strain-, charge-, and exchange bias-mediated modulations.[4-7] This material was predicted to have multiple properties, which can be exploited for many applications such as magnetic sensors and actuators, storage devices, and energy harvesting devices.[4–6]

One of the famous multiferroic composites which extensively developed is the multiferroic $BiFeO_3$-$CoFe_2O_4$ (BFO-CFO) nanocomposite. BFO-CFO nanocomposite has excellent magnetoelectric coupling and unprecedented physio-chemical properties showing emergent exotic fundamental physics.[8–10] BFO itself is a room-temperature single-phase multiferroic having the electric polarization originated from the lone pair of Bi^{+3} (s^2 orbital), while the magnetization is typically caused by Fe^{3+}.[3, 11] However, the magnetoelectric of BFO is relatively weak due to its antiferromagnetic with spin ordering of *G*-type originated from electron configuration of the half-filled d^5 orbital.[3, 11] On the other hand, the CFO is a ferrimagnetic material consisting of two different magnetic elements, Fe^{3+} and Co^{2+}, and it has very large magnetostriction compared to other magnetic materials except rare-earth ferromagnetic.[12] As depicted in Fig. 1, the ferroelectric (piezoelectric) properties of BFO and ferromagnetic (magnetostrictive) properties of CFO hold an important role in obtaining a strong magnetoelectric coupling, namely, magnetoelectric coupling *via* strain interaction.[8] In addition, a combination of BFO and CFO yields an antiferromagnetic-ferromagnetic exchange coupling and induces strong magnetic perpendicular enhancement.[13–15] The electric

field control ferromagnetism in the BFO-CFO can lead to many practical applications of next-generation electronic devices. Moreover, owing to distinctive photoactivity, small overpotential, as well as great stability in alkaline media, the BFO-CFO then possible to be utilized for the next photovoltaic, photocatalytic, and electrocatalysis devices.

BFO-CFO nanocomposite has been synthesized having many forms; nanoparticles, bulk, and single crystalline-like thin-film as described in Fig. 1.[16–23] Specifically, the single crystalline-like film can be found in several thin-film designs, such as multilayer (2-2 system), particulate-matrix (0-3 system), and pillars-matrix or vertically aligned nanocomposite (1-3 system). Thin-film holds a special place among other forms of multiferroic BFO-CFO nanocomposite. This is due to the fact that thin film is easier to integrate with electronic devices. In thin-film forms, the BFO-CFO can be utilized for various applications integrating active or passive devices.[24–26] The increasing demands on future electronics products utilizing multifunctional devices, particularly BFO-CFO based devices, compel researchers to develop the BFO-CFO by various thin-film architectures.[9, 14, 19–23, 27] In short, the exponential research and development of thin-film architectures of BFO-CFO nanocomposite nowadays make them close to their realization for practical applications.

More specifically, this review focuses on the exploration of BFO-CFO with a vertically aligned nanocomposite (VAN) thin-film system. It is simply because the BFO-CFO VAN is a unique system consisting of magnetoelectric, antiferromagnetic-ferrimagnetic, and structural couplings, which occur *via* large interface area interactions across the vertical surface between BFO and CFO phases, thus exhibiting emergent exotic properties.[8, 9] The exploration of BFO-CFO VAN is not limited to fundamental understanding but also how to optimize the physical properties of BFO-CFO VAN and thus open up new pathways toward practical applications. For instance, the development

of BFO-CFO VAN formation as well-organized two-dimensional (2D) CFO mesocrystals for bit pattern media application,[5] integration of BFO-CFO thin-film on flexible substrates[9] which can be developed for nanogenerator application,[6, 28] and controlling the shape of CFO pillars using various substrates to tune the magnetic anisotropy which importance for memory devices applications.[5, 21, 27] Henceforth, an overview of the recent progress and prospect of BFO-CFO VAN thin-film design is crucial to accelerate the development to reach the maturity level. Here, we discuss the fundamental understanding of the BFO-CFO VAN, the working mechanism, as well as the fabrication techniques. Moreover, the recent fabrication of the BFO-CFO VAN, which focuses more on the lab-scale sizes, delimit the commercialization of this material; hence, this present article not only addresses the prospects of next-generation devices based on BFO-CFO VAN but also identify the challenges and solutions to overcome the issues.

Recent forms and fabrications of BFO-CFO nanocomposite

Since BFO-CFO VAN was discovered in earlier 2000, this material has received significant attention up to now. BFO-CFO VAN can be fabricated using the self-assembled process *via* pulse laser deposition (PLD) method utilizing a single mixed BFO-CFO target.[29–31] As depicted in Fig. 2(a), when BFO and CFO phases simultaneously grow on the perovskite-type substrate, they could be constructed as a matrix and pillars or vice versa depending upon their energy surfaces on the substrate.[29, 30] In this manner, the surface energy anisotropy of both BFO and CFO phases plays an important role. The BFO has a rhombohedral crystal structure (point group *R3c*) with the perovskite-type, owing to a lattice parameter (a_{rh}) of 3.965 Å.[11] Meanwhile, the CFO has a cubic *Fd3m* spinel structure having a = 8.38 Å. CFO has almost double the unit cell of BFO, but the crystal structures and the oxygen

coordination similarities of both BFO and CFO phases make it possible to be epitaxially grown as BFO-CFO VAN on a single-crystalline substrate.[27, 29, 30]

The self-assembled process of BFO-CFO VAN can be understood by Winterbottom constructions, as shown in Fig. 2(b).[29, 30] Here, the perovskite substrate was used as a role model, owing to the necessity of achieving a cube-on-cube relation with BFO and CFO phases.[29, 30] The surface energy affects the wetting condition of BFO and CFO phases on the substrate, and thus further determines the matrix-pillars formation. The matrix is formed from the phase, which has smaller surface energy than the other or vice versa. For instance, the BFO fully wets while the CFO partially wets on a (001)-perovskite substrate, therefore the BFO forms as a matrix and CFO as pillars. Conversely, the CFO fully wets while the BFO partially wets on a (111)-perovskite substrate; consequently, the CFO forms as a matrix and BFO as a pillar.[29, 30] The observation of the self-assembled process using the wetting condition approach suggests that the self-assembled process is relatively insusceptible to the specific substrate ignoring the lattice mismatch. The BFO-CFO VAN was indeed can be grown on a wide range of perovskite substrates such as $LaAlO_3$ (LAO), $NdGaO_3$ (NGO), $SrTiO_3$ (STO), and $DyScO_3$ (DSO) substrates.[19, 21, 27]

The self-assembled matrix-pillars via a single process utilizing a single BFO-CFO target by a PLD technique is extensively used to fabricate BFO-CFO VAN due to its simple preparation and low-cost process. However, the significant vertical mismatch between matrix-pillars induces defects at the interfaces and further causes uncontrollable magnetic switching, which could become problematic for achieving stable memory devices.[5, 27] The self-assembled process using multiple targets is one of the excellent methods to modified and improve BFO-CFO VAN heteroepitaxy,[5, 32] as

schematically shown in Fig. 2(c). By using this method, the CFO phase is predicted to have better interconnection with the BFO phase.[5]

Nevertheless, it is found that the self-assembled BFO-CFO VAN fabricated *via* PLD method utilizing single or multiple targets leading to the uncontrollable location of the embedded pillars. In order to employ the BFO-CFO VAN for a device, it is important to control the embedded location of the pillars.[33] The existence of the embedded pillars then can be made in a well-ordered pattern by templating the self-assembly method.[18, 33] In principle, this method is started by patterning the substrate surface[18, 33, 34] using e-beam lithography into a square array, thus serving as a nucleation site of the embedded pillars.[18] A lithographic process is used to pattern an island on the substrate, as shown in Fig. 3(a).[18] This patterned layer then served as a template for the subsequent deposited BFO and CFO layer to forms a well-ordered BFO-CFO VAN.[18]

Even though the combination of BFO and CFO composite having a VAN system will produce a superior magnetoelectric coupling. However, when the BFO serves as a matrix and CFO as pillars, the leakage current in this BFO-CFO VAN system occurs. BFO is particularly ferroelectric material having large leakage current; thus, several attempts were conducted to decrease the leakage current in BFO, such as by doping.[35] In the BFO-CFO system, the leakage current leads to the degradation of ferroelectric properties[3, 11] since the BFO has inferior interconnection due to the existence of the CFO.[22] Therefore, another VAN architecture development is proposed, the so-called quasi (0-3) composite architecture as depicted in Fig. 3(b).[22] This system is a combination of layer-by-layer and VAN systems which is predicted to exacerbate net resistivity due to preferable interconnected BFO matrix, which enables to decrease of leakage current.[22] The quasi (0-3) BFO-CFO nanocomposite was achieved using the

PLD method by alternatively utilizing pure BFO and mixed BFO-CFO targets. A bottom BFO layer was deposited before the deposition of the BFO-CFO VAN layer; thereafter, it was continued by the deposition of the top BFO layer.[22] This architecture differs from the conventional particulate thin-film nanocomposite or 0-3 system since the obtained CFO filler is highly oriented as pillars embedded in a continuous BFO matrix.[22] In this configuration, excellent piezoelectric behaviour is obtained because the domain structures are not hindered by grain boundaries. Small-angle boundaries between grains in the sample also can improve strain coupling of BFO-CFO, thus, further enhance magnetoelectric coupling.[22]

Strain coupling between the constituent BFO and CFO phases is important to the magnetoelectric coupling mechanism.[9] Nevertheless, another issue related to the BFO-CFO VAN architecture is about the clamping effects originated from the substrate.[9, 20, 22] In the thin-film forms, the clamping effect is a common problem that decreases the magnetoelectric coupling, including in the BFO-CFO VAN system.[9] Even though the VAN system is predicted to have small clamping effects compare to planar system, however, the in-plane strain coupling of the vertical pillars is still constrained by the clamping effects from the substrate compared to ideally strain-free bulk geometry.[1, 3, 9, 36] Thus, an idea arises by synthesizing the so-called well-ordered BFO-CFO heterostructured nanodot arrays, as shown in Fig. 3(c).[20] In this configuration, the $SrRuO_3$ (SRO) bottom electrode was deposited before subsequent BFO and CFO. An ultra-thin nanoporous anodic alumina (AAO) membrane mask was used as a template to obtain a highly ordered BFO-CFO nanodot. This AAO has periodically ordered nanoscale pore size, thus the BFO, CFO, and SRO layers which were simultaneously deposited by using PLD method enable to forms of well-ordered nanodots BFO-CFO array on the substrate surface.[20] The well-ordered nanodots BFO-CFO can exhibit an

enhancement of magnetoelectric coupling because of the large atomic-level interface interaction and small substrate-clamping effect.[20]

The role of substrates

Instead of the abovementioned fabrication route development, the self-assembled BFO-CFO VAN architecture initially can be simply modified by strain engineering from the substrates.[19, 21, 27] A substrate holds a prominent role in determining the final design of BFO-CFO VAN, which further reflects its physical properties. The BFO-CFO VAN is particularly suitable to grow on perovskite substrates. Nevertheless, the BFO-CFO VAN growth also can be obtained on spinel, rocksalt oxide, Si substrates, as well as flexible substrates.[9, 27, 37, 38] Fig. 4 shows the schematic of BFO-CFO VAN architectures grown using various types of substrates. The shapes of embedded pillars depending upon the growth direction induced by wetting conditions and the strain-state among constituent phases and the substrates.[19, 21, 27, 29, 30, 39] Due to its lowest surface energy during epitaxial growth, the perovskite BFO has a tetrahedral equilibrium shape having {100} facets, while the spinel CFO has an octahedron equilibrium shape bounded by eight {111} facets, as shown in Fig. 4(a).[29, 30] When BFO has higher surface energy than CFO, the BFO partially wets on the substrate forming a pillar.[29, 30] This condition was found when BFO-CFO VAN grow on (110)- and (111)-STO substrates, wherein the BFO pillar emerges as stripe and triangular island, respectively, as shown in the Figs. 4(b) and 4(c).[23, 29, 30, 40] Similarly, when CFO has higher surface energy than BFO, the CFO partially wet on the substrate forming a pillar.[23, 29, 30, 40] This condition mostly could be found when BFO-CFO VAN grows on (100)-perovskite-type substrates, such as STO, LAO, NGO, and DSO.[19, 21, 41] For instance, The CFO pillars emerge as rectangular, stripe, and triangular island when it grows on

(100)-STO, DSO and NGO substrates, respectively, as shown in Fig. 4(d)-(f).[21] Specifically, the strain state among the constituent phases and the substrate hold an essential role in determining the shape of CFO pillars since the CFO more robust than the BFO from the epitaxial strain of the substrate.[14] A difference strain imposed from (100)-STO, DSO, and NGO substrates reflects the growth direction of the CFO phase; thus, they have different shapes of CFO pillars.[14, 21] However, when the lattice mismatch and the strain-state imposed from the substrate is too large, it can cause a large atomic dislocation and defect.[27] For instance, decomposition of the BFO phase is found when BFO-CFO grows on very large lattice mismatches such as $MgAl_2O_4$ and MgO substrates.[27] Larger lattice parameters of those substrates causing largely epitaxial tensile stress, and the Fe_xO_y, which have better lattice matching more favorable to be formed.[27] As a result, the Bi-rich dendritic structures at the film surface arise because of the decomposition of constituent phases.[27] Moreover, the utilization of buffer layer with relatively small lattice mismatch on the top of spinel, rocksalt oxide, Si, and flexible substrates then recently was used to obtain better growth formation of the self-assembled BFO-CFO VAN.[9, 37] The BFO-CFO VAN has recently successfully been fabricated on flexible mica substrate *via* the so-called quasi van der Waals epitaxy using CFO/SRO buffer layer.[9] The weak bonding between mica and the constituent phases leads to a decreasing in the substrate clamping effect.[9, 42] As a result, the magnetoelectric coupling in BFO-CFO VAN on mica was enhanced.[9]

Recent deposition techniques for BFO-CFO nanocomposites thin-film

As we explicitly mention along the time, the PLD technique is a prevalent route to obtain BFO-CFO VAN thin-film. However, the PLD system is limited to small film areas and sustain from inhomogeneity because of the narrow plume size of PLD.[3]

Therefore, there was recently developed the BFO-CFO VAN fabrication using sputtering and radio frequency (RF) magnetron sputtering which allows for homogenous large film deposition on a large size of the substrate.[43, 44] Fabrication of BFO-CFO VAN by sputtering can expand the horizon for large areas and scalable BFO-CFO VAN film. Recently BFO-CFO VAN has successfully grown on Nb:STO, STO-buffered Si, and LSMO/STO-buffered Si substrates using the sputtering technique.[43] Almost similar to that self-assembled growth by PLD, the BFO-CFO VAN by sputtering is formed *via* particles ejected from a bulk mixed BFO-CFO target due to a momentum exchange from energetic ions bombardment such as by Ar^{+}.[44] The vapor deposition process and sputtering growth conditions are important since the morphology and properties of BFO-CFO VAN depend on the kinetic factors such as the mobility of arriving species on the substrate surface.[43, 44] Moreover, the BFO-CFO nanocomposite has also successfully been fabricated *via* the chemical solution deposition method and sol-gel-assisted spin coating process.[45] In the spin-coating process, the mixed solutions of the BFO and CFO precursor enable nanoscale mixing of subsequent composite phases.[45] Similar to that BFO-CFO nanocomposite grown by physical vapor deposition; PLD, and sputtering, the BFO-CFO nanocomposite synthesized by chemical route shows adequate magnetic-electric properties.[45]

The forms and architecture development of BFO-CFO nanocomposite aims to enhance the magnetoelectric coefficient (α_{ME}). As depicted in Fig. 5, we compile the α_{ME} from various BFO-CFO nanocomposites and their comparison to the other magnetoelectric composite-related materials.[8, 9, 20, 22, 23, 46] The architecture of BFO-CFO VAN on the various substrate could affect the final properties as well as the magnitude of α_{ME}. The BFO-CFO core-shell has the largest α_{ME} which primarily because of the free from substrate clamping effect.[9, 20] Moreover, the modification of

the VAN architecture of BFO-CFO is not only to enhance the magnetoelectric coupling but also can modify the physical properties.[21, 36, 40] For instance, the magnetic anisotropy of BFO-CFO VAN could be changed by simply modify the orientation of the CFO phase using miss-orientation control by strain from the substrates.[21] It is also well-known that the BFO, which is highly strained induced by the substrates, has stronger piezoelectric properties compare to the unstrained BFO.[47, 48] The modification of architecture of BFO-CFO VAN will affect the magnetic and electric properties of individual BFO and CFO phases, thus, further, affect to the final magnetoelectric coupling. Yet, our unpublished results also indicate that the optical properties of BFO-CFO VAN also can be tuned by controlling the crystal structure of the BFO phase.[49] The exponentially increasing research and development of BFO-CFO VAN have reached the point where this material could be used for various applications. Here, we discuss the possible applications of BFO-CFO VAN in the next sections.

Applications of BFO-CFO nanocomposites

Magnetic sensors devices

Multiferroic BFO-CFO VAN is an attractive material for various electrically and magnetically couple devices such as a magnetic sensor.[2, 50–52] Magnetoelectric composite having various phase connectivity such as (0-3), (1-3), (2-2), or (1-1) have been tested for their feasibility as magnetic sensor devices.[53, 54] Magnetic sensor devices can be categorized according to their sensitivity to the degree of the measured magnetic fields, and their sensing ability strongly depends on the sensing mechanism.[51] For instance, Lorentz force-based and piezoelectric resonance-based sensors are used to detect high magnetic fields around 0.1 mT – 1 T.[51, 55, 56] The magnetoresistive and magnetoimpedance sensors are used to measure intermediate magnetic fields around 1 μT – 1 mT.[51, 57–59] The fluxgate magnetometers used to measure weak magnetic fields

around 0.1 nT – 100 μT.[51, 60–62] Superconducting quantum magnetometer utilizing the Josephson effect to measure ultra-low magnetic fields around 1 fT – 1 nT.[51, 59] An induction coil sensor is used to measure AC fields in the range of 10 fT – 1mT.[51, 63] The magnetic sensors employing magnetoelectric BFO-CFO VAN should be works for high and intermediate magnetic field sensors. The magnetoelectric-based magnetic sensors are possible to replace the Hall sensors which are largely used nowadays due to ultra-low power consumption operation.[64] Moreover, the magnetoelectric materials are also developed and possible to be utilized for magnetic sensors with sensitivity at Femto-tesla to pico-tesla at low frequency.[65–67]

It is well-recognized that both individual BFO and CFO phases are strong piezoelectric and magnetostrictive materials, respectively. Both BFO and CFO phase are strongly coupled induce strong magnetoelectric coupling. Therefore, direct and converse magnetoelectric effect (DME and CME) in BFO-CFO VAN is the origin for the application in the magnetic sensor. The strain-mediated magnetoelectric coupling as depicted in Fig. 6(a) explains how to realize magnetic sensor-based BFO-CFO VAN.[54] For the DME mechanism, the magnetic field can induce a strain because of the magnetostrictive effect in CFO. This strain is then transferred to the piezoelectric BFO across the large interface's area *via* structural coupling, and thus an electric polarization is generated due to the piezoelectric effects in BFO.[8, 9] The DME coupling outputs the voltage which is depending on the AC or DC magnetic field's magnitude, therefore it is possible to allow the BFO-CFO VAN to sense the field effectively. Moreover, the BFO-CFO VAN system also can be used for magnetic sensors utilizing CME.[68, 69] Here, an electric field which induce strain to the piezoelectric BFO is transferred to the magnetic CFO through the large interface area *via* structural coupling, creating the shape

modulation of CFO, and then, altering the magnetization easy axis of the magnetic CFO phase.[8, 9]

For the integration as magnetic sensor devices, the BFO-CFO VAN can be inserted in the electromagnetic coil bring a current I(t) as schematically depicted in Fig. 6(b). By using this structure design, the magnetoelectric-based sensor could suitable for DC magnetic field measurement in the at nano- to decades of mili-tesla, wherein, the output AC voltage u(t) is propagated due to the magnetoelectric effect.[51, 52, 70, 71] Here, the coil induces the AC magnetic field h(t) while the measured DC field H and the excitation field h(t) are imposed parallel to the plane of the sensor.[51] The applied magnetic field H and an excitation AC field activating the magnetostrictive CFO and induce the unipolar periodic strain.[8, 9] If a weak DC magnetic field is applied to the BFO-CFO VAN, the nonlinearity of the function leads to the formation of the periodic strain in the CFO phase. This deformation is then transferred *via* strain coupling to the piezoelectric BFO[19] and leads to the generated voltage u(t) with approximately the same time dependence.[51] Finally, the output voltage then is processed as a signal.

Moreover, since magnetoelectric materials can be developed for magnetic sensors with sensitivity at Femto-tesla to pico-tesla at low frequency,[65–67] the BFO-CFO VAN also could possible for the artificial magnetic sensor in the biomedical field. It has been reported that magnetic sensor-based magnetoelectric material could detect biomagnetic signals (~10^{-6} of the applied field in magnitude) in organ tissue such as a liver.[66] The magnetoelectric material is appropriate to be used in magnetic sensor application when their α_{ME} at least two order magnitude.[72–74] As shown in Fig. 5, the α_{ME} of BFO-CFO nanocomposite is high enough to be used as magnetic sensors. The α_{ME} is an important parameter determining the detection ability for magnetoelectric sensors[72] because the α_{ME} represents a relationship between the output electric field

and the input magnetic field.[72] Nevertheless, another sensor component, such as the circuit configuration is also essential, where the amplification of magnetic sensing depends on this configuration.[72] The magnetic sensor design as previously proposed could be one of a platform to obtain an efficient magnetic sensor-based BFO-CFO VAN.[70]

Memory devices

The existing transistor-based random access memory (RAM) technologies (flash, dynamic, and their derivatives) are facing their miniaturization limit.[75] Moreover, the rise of artificial intelligence (AI)-based applications nowadays demand ultra-high-speed, robust endurance, low-powered data storages to accelerate the complex computations which cannot be delivered by conventional memory technologies.[76] Henceforth, emerging nonvolatile memory technologies such as magnetic-based (MRAM), phase-change-based (PCRAM), ferroelectric-based (FeRAM), magnetoelectric-based (MERAM), and resistive-based (ReRAM) memories are being considered as the next-generation data storages; their reliable non-volatility behavior ensures long data retention (the ability to retain the stored information for more than a decade without consuming continuous power).[77]

More specifically, MERAM uses voltage/electric field manipulation to switch its state, called as voltage-controlled magnetic anisotropy (VCMA) effect.[78, 79] In comparison to current-controlled memory technologies such as spin-transfer or spin-orbit torques (MRAM), the VCMA requires much lower (if not free of) ohmic loss, lower switching current, and rendering high dense integration capability,[78] thus MERAM could realize energy-efficient data storage due to the low power operation.[78–82] Here, we foresee the potential of the magnetoelectric properties of BFO-CFO VAN

for fabricating high-performance low-powered MERAM device; BFO-CFO VAN, as the magnetoelectric layer, can be integrated with a magnetic tunnel junction (MTJ) device (reference layer – tunnel barrier – free layer), as depicted in Fig. 7(a).[83] In this configuration, a BFO-CFO VAN layer can be used to control the magnetization of the MTJ by the electric polarization.[83–86] The bit is stored by the magnetization direction of the references layer, read by the resistance of the MTJ, and thus written by applying a voltage across the magnetoelectric BFO-CFO VAN layer. When the magnetization of the references layer is coupled to the spins on the magnetoelectric BFO-CFO VAN layer, the ferroelectric polarization *P* in the magnetoelectric BFO-CFO VAN layer can modulate the magnetization configuration of the free layer and reference layer in the MTJ from parallel to antiparallel, and *vice versa,* and induce the resistance changes.[83]

In addition, since BFO-CFO VAN can consist of nanomagnetic CFO mesocrystals (pillars), therefore, it can be used for bit pattern media (BPM) applications, as schematically shown in Fig. 7(b).[5] In this configuration, each of the isolated CFO pillars nanomagnet can be programmed to store 1-bit of information that is read by a recording head.[87–89] A recent report using a high sensitivity dynamic cantilever magnetometry (DCM) was showing strong magnetic anisotropy of a single CFO mesocrystals in the BFO-CFO VAN system.[5, 90] Therefore, the BFO-CFO VAN having CFO mesocrystals are suitable for BPM application from the anisotropy field point of view.[5] The magnetic anisotropy of the single CFO mesocrystals can be controlled by a voltage pulse/bias via ferroelectricity of BFO matrix, then an efficient magnetic switching via magnetoelectric coupling can be achieved (VCMA effect).[78] The BFO-CFO VAN opens up an avenue for exploration of new material and design for BPM applications. Nevertheless, Further study is required to obtain highly efficient BFO-CFO VAN-based BPM; one of the possible approaches is to modulate the

magnetic switching field distributions and bit information writing via the good arrangement of CFO pillars.[87] Such a well-designed pattern arrangement can be realized by utilizing the lithography technique as mentioned in the previous section. Moreover, the magnetic anisotropy of the CFO pillar can be further improved to obtain even more efficient magnetic switching; it is observed that the magnetic anisotropy of CFO can be modified by using strain control from the substrate and doping.[91–95]

Energy harvesting devices

Nowadays, the developing flexible materials has become mainstream research topics to obtain next generation flexible devices.[96–99] This development not only to discover new class of flexible materials, but the idea also could be related to obtain new method how to transform a thin-film which previously found in rigid forms into a flexible thin-film then further could be utilized for flexible devices.[100–103] Recently, BFO-CFO VAN has successfully transformed into flexible thin-film using mica substrate as shown in Fig. 8(a). In the present approach, the BFO phase was formed as pillars, while the CFO phase was a matrix as shown schematically in Fig. 8(b).[9] The BFO-CFO VAN was fabricated on a 2D layered mica substrate results in an unconstrained film due to the van der Waals (vdW) epitaxial relationship which can significantly reduce the substrate clamping effect.[9] This feature is essential to obtain large piezoelectric and magnetostrictive response, and thus further increase the magnetoelectric effect in the BFO-CFO VAN system.[9, 104] The BFO-CFO VAN thin film on flexible mica substrate then can be used for flexible devices having distinctive set of features; lightweight, stable at high temperatures, and chemically inert.[9, 102, 104]

One of the possible next-generation flexible devices that can be achieved utilizing flexible BFO-CFO VAN is energy harvesting devices; the so-called magneto-

mechano-electric (MME) generators.[6, 105] The MME exploits low-frequency magnetic fields to generate power, thus possible to be integrated as wireless power transfer device for operating the Internet of Things (IoT) devices.[106] The MME generators is deliberated to resonate at a fixed frequency of weak AC magnetic fields through flexible magnetoelectric materials such as BFO-CFO VAN to generate energy and electricity.[6, 106] BFO is considered a magnetoelectric material which possible to integrated as nanogenerators devices. It was reported previously that BFO thin-film grow on flexible Ni tapes possesses a piezoelectric and saturation polarization coefficient of 52 pm/V and 69 μC/cm^2,[107] respectively. This value is comparable with well-known ferroelectric $BaTiO_3$ which can generate energy with a voltage output about ~10 V and a current density of ~1.2 μA cm^{-2}.[108, 109] However, the BFO on the flexible Ni substrate was reported to exhibit a small α_{ME} about 3.5 mV/cm.Oe, which much smaller than reported BFO-CFO VAN on a flexible mica substrate.[9] Therefore, BFO-CFO VAN should be much more possible to be integrated as MME devices due to its strong magnetoelectric coupling.

In the BFO-CFO VAN on flexible mica reported previously, the out-of-plane converse piezoelectric coefficient (d_{33}) of existed BFO pillars is altered when the sample is under mechanical strain due to the changes of polarization rotation induced by the alteration of the BFO pillars length along the *c*-axis.[9] The result also shows that the obtained α_{ME} values of flexible BFO-CFO/mica under mechanical strain are still comparable with that obtained in unclamped magnetoelectric composite and higher than BFO-CFO VAN on a rigid substrate.[20, 46] Fig. 8(c) showing the schematic of the application of flexible magnetoelectric BFO-CFO VAN for energy harvesting devices utilizing magnetic noise which acts as an AC magnetic field. We speculate that strong magnetoelectric coupling in flexible BFO-CFO VAN can create an electrical charge

when induced by even with the small magnetic field. The magnetoelectric effect in the flexible BFO-CFO VAN resulting in multiple energy transduction as sequential interaction of MME generation; starting from magnetic energy into mechanical energy and finally produce electrical energy.[6] When the AC magnetic field is applied to flexible BFO-CFO VAN thin-film, the magnetostrictive CFO reacted by either expanding or shrinking (magneto-mechano coupling) and simultaneously induce the piezoelectric BFO *via* structural coupling. This coupling creates an output voltage from the electrical load *via* a direct piezoelectric effect (mechano-electric coupling), thus generate the electric power that can be stored/used for device operation.[6]

Discovering new flexible magnetoelectric materials and/or transforming a thin-film that was previously found in rigid substrate into flexible thin-film is essential for developing MME devices.[28, 100] For MME applications, magnetostriction, piezoelectric, and magnetoelectric coupling hold important roles in energy conversion between magnetic and electric domains.[106] MME based on various piezoelectric and magnetoelectric is reported for effective power generation.[110] Thus, selecting a material having large d_{33} and α_{ME} is important. In general, flexible material having d_{33} of ~30-100 pm/V such as ferroelectric polymers and lead-free ferroelectric $BaTiO_3$ is enough to be integrated for nanogenerator devices.[110–112] This value is comparable with that reported BFO-CFO VAN on flexible mica substrate having 76.5 pm/V. Indeed, this BFO-CFO/mica has a much lower d_{33} compare to $Pb(Zr,Ti)O_3$ (PZT) having an remarkably efficient piezoelectric energy conversion owing high d_{33} of about ~250 pm/V.[113] Nevertheless, the large magnetoelectric coupling of BFO-CFO VAN could be used in MME where multiple energy transduction of magnetic-mechanic-electric is available in flexible BFO-CFO VAN thin-film. Moreover, CFO has very large magnetostriction comparing to other magnetic materials, except rare-earth

ferromagnetic.[12] Therefore, a combination of BFO and CFO phases having a VAN system could generate a strong magnetoelectric coupling that eventually could generate self-induced energy for MME devices.

Other applications: photovoltaic, photocatalyst, and photoelectrochemical devices

A recent report shows that the photovoltaic effect can be increased and controlled by the ferroelectric and magnetic response.[114] In ferroelectric materials, electric polarization enhances the photovoltaic effect and ferroelectric domains can separate the photon-generated charge carriers.[114] Whereas, in magnetic materials, the magnetic order can mitigate the flow of photocurrent because of the existence of spin-orbit interaction and magnetic domain arrangement.[114] In the BFO system, the tenable J_{sc} and V_{oc} confirm the prominent factors of the polarization-induced electric field in the photovoltaic system.[115] As for CFO, this material is an *n*-type ferromagnetic-semiconductor potential for magnetic field tuning of the photoelectrochemical properties. CFO has high magnetostriction behavior, high-rate strain modulation with the magnetic field, moderate saturation magnetization, the optical bandgap in the range of visible light region, and the ability of magneto-tunable photocurrent.[116–121]

A combination of CFO with BFO phases as BFO-CFO VAN thin film can be implemented for magnetophotovoltaic devices; tunable photovoltaic with the magnetic field.[122] The previous report shows that the magnetic field can modulate the photovoltaic effects in multiferroic CFO/Pb(Zr,Ti)O_3 nanocomposite thin-films; the J_{sc} and V_{oc} decreases with increasing the magnetic field.[122] However, to the best of our knowledge, no recent study about the photovoltaic based on BFO-CFO VAN. The photovoltaic effects in the combination of BFO and CFO phases as BFO-CFO VAN will be interesting to study and, eventually, to be integrated as magnetophotovoltaic

devices. As we can expect, the ferroelectric-driven enhancement of photovoltaic in the BFO phase could be controlled by a magnetic field *via* magnetic coupling with the CFO phase. In addition, the BFO-CFO VAN structure offer large coupling across the vertical interface between BFO and CFO phases that could induce strong magnetic induce tunable photovoltaic devices. BFO-CFO VAN layer can be inserted in various types of the commercial solar cell devices, such as wafer and thin-film-based, or the other existed perovskite-based and dye-sensitized-based solar cells. In this case, BFO-CFO VAN layer can enhance the photovoltaic effect by electric polarization in BFO phase, while the ability of magneto-tunable photocurrent in CFO could possible to tune the photocurrent generated in the solar cell heterojunctions.

Both BFO and CFO phases are also great potential to be developed in photocatalyst applications. Among various photocatalyst materials that have been tested, BFO is a foremost multiferroic material having superior spontaneous polarization and considered as one of the potential ferroelectrics material for photovoltaics, photocatalyst, and photoelectrochemical (PEC) water splitting because of its narrow bandgap and good chemical stability.[123] On the other hand, CFO has tunable magnetic properties and high absorption capability.[124] CFO also offers excellent reusability considering the easy magnetically photocatalyst material separation.[125] Therefore, a combination of BFO and CFO phases is an ideal material for photocatalyst applications. It has been reported that the core-shell magnetoelectric BFO-CFO nanocomposite nanoparticles capable to initiate an electrochemical process under the applied magnetic fields which enable to decrease of organic pollutants such as rhodamine B (RhB) by up to 97% within 50 minutes.[10]

Even though that the former results show in BFO-CFO nanoparticles, nevertheless, BFO-CFO VAN thin-film should be appropriate for photocatalyst

applications, such as for wastewater treatment plants. It is because the surface facet of the thin-film is essential for molecular adsorption.[126–128] Thin-films is suitable to be utilized on an industrial-scale photocatalyst device and it mitigate the handling of photocatalytic materials in several sectors; a suitable design which adaptable in the reactors, recovery, recyclability, etc.[129] Moreover, the activity of the catalysts in the thin-film forms is reported higher by an order of magnitude due to maximation of specific surface area utilization compare to in the particulate form.[127] With larger-sized thin-film, the catalyst effect could be higher than that found in the particulate form in the liquids because the particulate forms may suffer from the light absorption, and thus caused light scattering rather than absorption.[127] Therefore, the photocatalysts' thin-film is predicted leading to cost-effective hydrogen production due to the few amount of material utilization and minimum equipment.[127]

Similar to the magnetic field-enhanced photocatalysis process, the induction of magnetic field to the electrocatalysis process has been emerged as a promising and novel strategy to improve the electrochemical reaction-driven catalytic process, overcoming the bottle-neck stage of intrinsically modified electrocatalyst materials.[130] BFO has recently shown a promise for photoelectrochemical water splitting owing to the large and stable spontaneous ferroelectric polarization, enabling the high charge carrier separation *via* depolarization electric field. More notably, large open-circuit potential upon the band-gap limit can be achieved. Therefore, BFO is receiving much attention for next-generation electrodes.[131–134] Although showing an excellent result, improvement has to be done to maximize the electrocatalysis performance. For instance, loading the highly active co-catalysts based on Pt, Pd, Au, Ag, Ir, and Ru.[135–137] However, precious metals are prone to resource scarcity, limiting to cost-effective and large-scale industrial realization. Instead, BFO can alternatively be combined with the

CFO. In this regard, CFO has a comparable low overpotential to the RuO_2 and IrO_2 electrocatalyst, which is required as a bifunctional catalyst to drift OER and ORR.[138, 139] More specifically, rGO/CFO exhibited a small overpotential of 780 mV,[10] CFO/CNTs hybrid has the onset potential of 480 mV at 10 mA cm^{-2} current density,[140] and CFO/biocarbon nanocomposites reached an onset potential of 460 mV at 17.7 mA cm^{-2}.[141]

Neither BFO-CFO bulk composite nor BFO-CFO VAN has been explored for electrocatalyst electrode. Nevertheless, having in mind that electrocatalytic properties of the composite may be predicted taking advantage of the individual component. A large spin polarization has been theoretically and experimentally verified in magnetic spinel oxide CFO thin-film[142, 143] and therefore CFO becomes an electro-active catalyst, especially for OER and ORR. Meanwhile, spontaneous electrical polarization, which BFO possesses, is beneficial for the acceleration drift and separation of charge carriers, although its small ferromagnetism could limit the HER process. As aforementioned, a strong magnetoelectric coupling *via* strain interaction in the BFO-CFO induces strong magnetic enhancement, spin polarization, and controllable ferromagnetism. In this manner, BFO serves as an external spin polarization and charge carrier separator for CFO, while CFO acts as the active catalyst for BFO. Thus, the coupling of BFO with CFO may enhance the HER, OER, and ORR. Previous research showed how the external magnetic field could further enhance the electrocatalytic performance of catalyst materials for HER, OER, and ORR. Generally, when the applied magnetic field act to the conventional three-electrode reactors, the indirect effect from Lorentz force that perpendicular to the motion of mass and gas bubbles can modulate the rate of the electrocatalytic process.[144] The applied high-frequency alternating magnetic field also responsible for the localized heating of the catalyst so-called hyperthermia-promoted

catalysis which increased the reaction rate in the HER.[145] It was suggested that a magnetic field, either external or internal, is favorable for the paramagnetic spin alignment of the molecular oxygen during the reaction analogous to the chiral system in OER. Inspired by these emerging results, BFO-CFO indeed needs special attention for the exploitation of their promising properties as magnetic-electrode for electrocatalysis devices.

Challenge, solutions, and prospects of BFO-CFO nanocomposite

In general, the BFO-CFO VAN is considered to have a complicated fabrication process and thus it requires high installation costs and might hinder market growth, despite its rise in demand and increasing interest for the aforementioned variety of device applications.[4, 146] On the other hand, there is an urgent need for the adoption of some electronic devices in many real-life applications, in which the BFO-CFO VAN might contribute better along with the development of technologies especially nowadays. For instance, in the near future, the IoT seems to be developed more widely and becomes important for human life aligned with the industrial revolution 4.0 to create a smart living as a trending lifestyle to live a better life through the envision of lower energy consumption.[147, 148] To get along with the development of more sophisticated technologies in the IoT era, it also requires smart materials to achieve it. Various advanced materials technology has been developed including the fact that BFO-CFO VAN could also be possibly be integrated into next-generation devices to support the IoT. BFO-CFO VAN also covers many applications in biomedical sensors, energy, and the environment as we mentioned in previous sections.

Utilizing BFO-CFO VAN for magnetic sensor devices may replace the Hall sensors which are largely used nowadays due to ultra-low power consumption

operation.[64] Since magnetoelectric materials can be developed for magnetic sensors with sensitivity at Femto-tesla to pico-tesla at low frequency,[65–67] the BFO-CFO VAN also could possible for the artificial magnetic sensor in the biomedical application. However, it has the challenge to largely improve the magnetoelectric coupling of BFO-CFO VAN so that it can be utilized for magnetic sensor detection from nano-tesla up to decades of milli-tesla ranges. To overcome this issue, the fabrication process which keeps the high crystallinity of BFO-CFO VAN is necessary because the better interfacial coupling between BFO and CFO phases could induce large magnetoelectric coupling. Another sensor component such as the circuit configuration which can amplify the magnetic sensing is important to be developed since the sensing ability is depending on this configuration.[72] Improving the magnetic sensor design could be one of the good avenues to obtain efficient magnetic sensor-based BFO-CFO nanocomposite.[70]

Furthermore, the magnetoelectric coupling of the BFO-CFO could generate energy-efficient of memory devices, therefore it can replace conventional memory devices that we currently have in the market; volatile memory, such as static and dynamic RAM. The MERAM can realize the high-speed and high-capacity memory. It is important to note that the non-volatile RAM such as MRAM was commercialized in 2019, by considering the BFO-CFO-based MERAM configuration is similar to MRAM and MERAM fabrication is CMOS compatible process, thus, it brings promise to integrate this technology with the current CMOS system in the near future. Nevertheless, in device level perspective, the limitation of BFO-CFO VAN for memory devices is that controlling the location of CFO pillars is necessary for magnetic switching field distributions and bit information writing; once we overcome this challenge, the BFO-CFO VAN not only can be used for MERAM, but also for BPM

applications.[87] Well-ordered CFO pillars can be achieved by fabrication methods utilizing well-ordered pattern and lithography. In fact, this method is a common fabrication process in the wafer fab. Thus, it is possible to fabricate BFO-CFO VAN for mass production for memory devices using a well-ordered pattern and lithography methods. Moreover, the magnetic anisotropy of the CFO pillar is also necessary to be improved to obtain efficient magnetic switching. The magnetic anisotropy of CFO could be modified by using strain control from the substrate and by doping.[91–95]

Dependency over mobile electronic devices increases rapidly along with the strong need to develop smart devices using sensors, wearable, and battery-less devices in the IoT era to sustain an aging society.[149] The BFO-CFO VAN also has prospects to be utilized for mobile electronic and energy harvesting devices. Nevertheless, it has a challenge in searching for a proper substrate, in particular, a flexible substrate that enables it to be used for growing high-quality BFO-CFO VAN. Flexible mica is the only possible substrate so far, since it has good crystallinity, flat atomically surface, chemically inert, and can withstand high temperature. The prospect for flexible BFO-CFO VAN could be possible for MME to enable self-generated power using low-frequency magnetic fields. According to European Commission,[150] the global energy harvesting market has been experiencing explosive growth since 2014 and has been anticipated to keep increasing in the coming years.[150] It implies that BFO-CFO VAN may also have a huge potential to be a part of the explosive growth of energy harvesting to power the implementation of the IoT era shortly. Power generation is responsible for driving IoT devices, especially to enable the development of technologies with economic and technological impacts in terms of autonomous power supply.[151]

In addition to energy harvesting, materials from environmental sources, such as photovoltaic materials, contribute 12% to the global energy harvesting technology in

2014. The European Commission has predicted that it might keep increasing by 26% in the forthcoming years from the technology development using solar energy that utilizes photovoltaic materials in commercial applications, such as chargers for electronic devices. There is also a prospect for BFO-CFO VAN to be used for photovoltaic-powered sensors to facilitate the rapid spread and growth of IoT devices. Powering sensor networks that utilize this material could also be essential to connect and coordinate IoT devices, hence numerous sensors are required and thus BFO-CFO has a huge potential for mass utilization if it could be produced in mass production. Large area devices are very significant to achieve high efficiency and large electricity generated by light. However, the main challenge of utilizing BFO-CFO VAN for photovoltaic devices is in its limited scale for fabrication.

Technically, the photovoltaic effect can be improved by electric polarization while ferroelectric domains in the BFO can separate the photon-generated charge carriers.[114] On the other hand, the magnetic order of CFO can support the flow of photocurrent because of domain arrangement and spin-orbit interaction.[114] Therefore, BFO-CFO VAN could be used for magnetic induce photovoltaic in solar cells devices having strong photovoltaic effects. This feature have not be seen in well-known and commercialized solar cells devices nowadays such as Si-based, perovskite, and CIGS solar cells devices.[152] Hence, the integration of BFO-CFO VAN layer in those of solar cells could realize the next-generation solar cells devices. Moreover, abundant resources of iron, cobalt, and bismuth should have a much lower price compared to silicon-based and indium-based photovoltaic devices.[152] The utilization of BFO-CFO VAN layer could decrease material usage and the layer thickness of the main solar cells layer such as CIGS solar cells having high-priced In and Ga element, thus it can be a solution for the lack of commercialization of CIGS-based solar cells because the price issue.[152] The

stable chemical compound of BFO-CFO VAN also makes it better than perovskite-based solar cells devices.[153] Therefore, it emphasizes how BFO-CFO VAN may have a huge prospect toward the rapid spread and growth of IoT applications utilizing self-powered devices such as solar cells.

Another potential utilization of the BFO-CFO VAN is for magnetic field-induced electrocatalyst devices. The challenge for this implementation is that it needs special electrolyzer designs for convenient exploitation. Hence, selecting a proper electrolyzer design which also suitable for mass fabrication is required to overcome the challenge. In another case, the utilization of BFO-CFO VAN thin-films for magneto-photocatalyst devices has potential on the industrial scale; simple and convenient design, adaptability in the reactors, recyclability, recovery, etc.[129] The magneto-photocatalyst effect in BFO-CFO VAN thin-film materials may be larger than that of the particulate form in solutions. However, a large-scale area of the film is required and it becomes a challenge to utilize this material for photocatalyst devices. To reach large-scale fabrication of the BFO-CFO VAN, a sputtering method and non-vacuum thin film fabrication method could be implemented. The latter offers a low cost for the large-scale area of thin-film fabrication.[152] Regarding all the aforementioned discussion in this section toward the utilization of the BFO-CFO VAN material, to the best of our knowledge, the limitation of BFO-CFO VAN for mass production is mostly related to the fabrication process. Looking at how prospective BFO-CFO VAN can contribute to the future IoT era, the limitations of this material for several applications are also discussed in this review paper.

The biggest market potential for BFO-CFO VAN is our human population since more people incorporate technology into their daily lives, including the rapid interest in IoT. This change increases including the demand for magnetic sensors and memory

devices. Magnetic sensors are widely used in consumer electronics such as smartphones and tablets, and the automotive industry such as accelerometers and position sensors. As for smartphones, the number of users increases from the year 2016 to 2019 and forecast until the year 2021.[154] When the number of smartphone users exponentially increases, the demand for smartphones is also increasing since companies keep updating their smartphone products. From this smartphone industry alone, we can predict that there will be greater demand for BFO-CFO VAN material in the future. BFO CFO VAN also has strong potential demand in the smartphone market since it is also using memory devices. Memory devices are everywhere from smartphones, cameras, tablets, computers, smartwatches, smart tv, and so on. According to Markets and Markets, a market research and consulting company, the global market size of electronics devices will reach USD 135.3 billion in 2025 from USD 78.3 billion in 2020.[155]

Moreover, as pollution gets higher and the global air quality gets worse, the demand for clean energy is increasing. One of the main renewable sources of clean energy is solar photovoltaic or photocatalyst devices. It is recorded an increasing capacity more than twice during 2015-2018 for the global cumulative installed solar photovoltaic to approximately 509,000 megawatts[156] with a total worth of USD 52.5 billion in 2018 and is projected to reach USD 223.3 billion in 2026s.[157] Since the BFO-CFO can be implemented for photovoltaic devices, it is more likely that the demand for this material will be exponentially increasing following the demand for the solar photovoltaic system to support the rapid growth of the IoT era. According to how the market will keep growing toward the IoT era, it might be worthwhile to consider the BFO-CFO VAN material in various types of sensors, memory, and photovoltaic devices for any IoT applications in the near future. Thus, the global interest in technology,

especially in IoT products, surely expands the potential market for the BFO-CFO materials.[158, 159]

Other than IoT applications, the BFO-CFO VAN shows some potential for environmental and biomedical applications. More diverse diseases are linear to the increase of global pollution. Perennial health problems such as cancer need to be tackled and imaging analysis becomes the mandatory technique to evaluate this disease. Here, we can exploit the BFO and CFO phases for biomedical imaging owing to their excellent optical and magnetic properties, where non-invasive photon energy is absorbed, and the magnetic field is applied to control the direction of the nanocomposite to the targeted cancer cells. Moreover, BFO has shown less cytotoxicity, good haemolytic response, and good biocompatibility; therefore, it may be a safe material for various human tissues.[160] Furthermore, there is an urgent demand for antibacterial and antiviral coatings to kill infected fomites in health care facilities. In the recent SARS-CoV-2 pandemic, surfaces have become one of the mediums for widespread infection. CFO has long been investigated for its antibacterial activity, particularly against multidrug-resistant clinical pathogens (Gram-positive bacteria *S. epidermidis* ATCC 1228 and Gram-negative bacteria *E. coli* ATCC 8739).[161] The antibacterial mechanism is attributed to the formation of reactive oxygen species and the crystal surface abrasive texture upon UV-light irradiation. Since the BFO exhibits remarkable photocatalytic activity, it is expected to show an equal photocatalytic antibacterial performance. A recent study has demonstrated the capability of BFO to inhibit the growth of bacteria such as *E. coli*, *S. aureus*, and *E. faecalis*.[162] BFO-CFO, in the form of nanocomposite film, can be potentially utilized as nanocoating of various objects and substrates (metals, polymers, ceramics, papers, and textiles/fibers) in health care facilities. Therefore, a simple, low-cost, efficient, environmental-friendly, and biocompatible

surface cleaning can be performed to replace the *state-of-the-art* surface disinfectant process, which may result in multidrug-resistant bacteria.

Conclusions

Multiferroic BFO-CFO VAN thin-film has attracted great attention in the last decade due to their predominance of multiple properties; magnetic, electric, and optic. BFO and CFO phases are individually exhibited excellent physical and chemical properties. Thus, in the combination of BFO and CFO in VAN thin-film forms having large interface interactions, BFO-CFO is predicted can be utilized for next-generation devices. Various modifications on this material through various fabrications have been done. This is including architecture design to enhance the functionality of BFO-CFO VAN, as well as various vacuum- and non-vacuum-based deposition methods used to fabricate BFO-CFO VAN. Low-cost fabrications technique and the methods that enable the synthesis of a large-scale area of the materials are the main challenges for the realization and commercialization of BFO-CFO VAN-based devices. We may mention that the sputtering method is appropriate among other fabrication techniques that can be used for the realization of BFO-CFO VAN-based devices for commercialization because sputtering was widely used for semiconductor devices so far. In any case, a proper choice of the substrates, especially flexible substrate, is also important to generate the functionality of BFO-CFO VAN for any device.

From the exponential explorations, this material possible to be integrated for many applications, including contribution in many devices for the coming years, since the potential market for the BFO-CFO VAN thin-films is wide. Strong magnetoelectric properties of BFO-CFO VAN enabled to sense of femto-tesla to pico-tesla of the magnetic field at low frequency; therefore, they can be used for next-generation

magnetic sensors. The strong magnetoelectric properties of BFO-CFO VAN also can be utilized to create memory and energy harvesting devices that could be integrated into IoT applications. Whereas, as the BFO and CFO phases possess distinctive optoelectronic and optochemical properties, therefore they can be integrated with photovoltaic and photo-electrocatalyst devices. Here, we summarize recent fabrications and possible applications of BFO-CFO VAN in Table 1.

References

[1] Martin, L. W.; Crane, S. P.; Chu, Y. H.; Holcomb, M. B.; Gajek, M.; Huijben, M.; Yang, C.-H.; Balke, N.; Ramesh, R. Multiferroics and Magnetoelectrics: Thin Films and Nanostructures. *J. Phys.: Condens. Matter*, **2008**, *20* (43), 434220. https://doi.org/10.1088/0953-8984/20/43/434220.

[2] Hu, J. M.; Nan, C. W. Opportunities and Challenges for Magnetoelectric Devices. *APL Mater.*, **2019**, *7* (8), 080905. https://doi.org/10.1063/1.5112089.

[3] Martin, L. W.; Chu, Y. H.; Ramesh, R. Advances in the Growth and Characterization of Magnetic, Ferroelectric, and Multiferroic Oxide Thin Films. *Mater. Sci. Eng. R*, **2010**, *68* (4–6), 89–133. https://doi.org/10.1016/j.mser.2010.03.001.

[4] Ortega, N.; Kumar, A.; Scott, J. F.; Katiyar, R. S. Multifunctional Magnetoelectric Materials for Device Applications. *J. Phys. Condens. Matter*, **2015**, *27* (50), 504002. https://doi.org/10.1088/0953-8984/27/50/504002.

[5] Guo, S.; Xu, F.; Wang, B.; Wang, N.; Yang, H.; Dhanapal, P.; Xue, F.; Wang, J.; Li, R.-W. 2D Magnetic Mesocrystals for Bit Patterned Media. *Adv. Mater. Interfaces*, **2018**, *5* (21), 1800997. https://doi.org/10.1002/admi.201800997.

[6] Ryu, J.; Kang, J. E.; Zhou, Y.; Choi, S. Y.; Yoon, W. H.; Park, D. S.; Choi, J. J.; Hahn, B. D.; Ahn, C. W.; Kim, J. W.; et al. Ubiquitous Magneto-Mechano-Electric Generator. *Energy Environ. Sci.*, **2015**, *8* (8), 2402–2408. https://doi.org/10.1039/C5EE00414D.

[7] Chu, Z.; PourhosseiniAsl, M.; Dong, S. Review of Multi-Layered Magnetoelectric Composite Materials and Devices Applications. *J. Phys. D*, **2018**, *51* (24), 243001. https://doi.org/10.1088/1361-6463/aac29b.

[8] Oh, Y. S.; Crane, S.; Zheng, H.; Chu, Y. H.; Ramesh, R.; Kim, K. H. Quantitative Determination of Anisotropic Magnetoelectric Coupling in $BiFeO_3$–$CoFe_2O_4$ Nanostructures. *Appl. Phys. Lett.*, **2010**, *97* (5), 052902. https://doi.org/10.1063/1.3475420.

[9] Amrillah, T.; Bitla, Y.; Shin, K.; Yang, T.; Hsieh, Y. H.; Chiou, Y. Y.; Liu, H. J.; Do, T. H.; Su, D.; Chen, Y. C.; Jen, S. U.; Chen, L. Q.; Kim, K. H.; Juang, J. Y.; Chu, Y. H. Flexible Multiferroic Bulk Heterojunction with Giant Magnetoelectric Coupling *via* van Der Waals Epitaxy. *ACS Nano*, **2017**, *11* (6), 6122–6130. https://doi.org/10.1021/acsnano.7b02102.

[10] Mushtaq, F.; Chen, X.; Torlakcik, H.; Steuer, C.; Hoop, M.; Siringil, E. C.; Marti, X.; Limburg, G.; Stipp, P.; Nelson, B. J.; Pane, S. Magnetoelectrically Driven Catalytic Degradation of Organics. *Adv. Mater.*, **2019**, *31* (28), 1901378. https://doi.org/10.1002/adma.201901378.

[11] Catalan, G.; Scott, J. F. Physics and Applications of Bismuth Ferrite. *Adv. Mater.*, **2009**, *21* (24), 2463–2485. https://doi.org/10.1002/adma.200802849.

[12] Brabers, V. A. M. Chapter 3 Progress in Spinel Ferrite Research. In *Handbook of Magnetic Materials*; Elsevier, 1995; Vol. 8, pp 189–324. https://doi.org/10.1016/S1567-2719(05)80032-0.

[13] Chen, Y. J.; Hsieh, Y. H.; Liao, S. C.; Hu, Z.; Huang, M. J.; Kuo, W. C.; Chin, Y. Y.; Uen, T. M.; Juang, J. Y.; Lai, C. H.; et al. Strong Magnetic Enhancement in Self-Assembled Multiferroic-Ferrimagnetic Nanostructures. *Nanoscale*, **2013**, *5* (10), 4449. https://doi.org/10.1039/c3nr00104k.

[14] Amrillah, T.; Chen, Y.-X.; Duong, M. N.; Abdussalam, W.; Simanjuntak, F. M.; Chen, C. H.; Chu, Y. H.; Juang, J. Y. Effects of Pillar Size Modulation on the Magneto-Structural Coupling in Self-Assembled $BiFeO_3$–$CoFe_2O_4$ Heteroepitaxy. *CrystEngComm*, **2020**, *22* (3), 435–440. https://doi.org/10.1039/C9CE01573F.

[15] Amrillah, T.; Juang, J. Y. Magnetic Saturation Enhancement in the Vertically Aligned Multiferroic Nanocomposite Thin Film. *AIP Conf. Proc.*, **2020**; 2314, 020011. https://doi.org/10.1063/5.0034130.

[16] An, F.; Zhong, G.; Zhu, Q.; Huang, Y.; Yang, Y.; Xie, S. Synthesis and Mechanical Properties Characterization of Multiferroic $BiFeO_3$-$CoFe_2O_4$ Composite Nanofibers. *Ceram. Int.*, **2018**, *44* (10), 11617–11621. https://doi.org/10.1016/j.ceramint.2018.03.235.

[17] Budi, M. A. K.; Glass, E. B.; Rudawski, N. G.; Andrew, J. S. Exchange Bias in Bismuth Ferrite/Cobalt Ferrite Janus Nanofibers. *J. Mater. Chem. C*, **2017**, *5* (33), 8586–8592. https://doi.org/10.1039/C7TC00975E.

[18] Comes, R.; Liu, H.; Khokhlov, M.; Kasica, R.; Lu, J.; Wolf, S. A. Directed Self-Assembly of Epitaxial $CoFe_2O_4$–$BiFeO_3$ Multiferroic Nanocomposites. *Nano Lett.*, **2012**, *12* (5), 2367–2373. https://doi.org/10.1021/nl3003396.

[19] Amrillah, T.; Vandrangi, S. K.; Bitla, Y.; Do, T. H.; Liao, S. C.; Tsai, C. Y.; Chin, Y. Y.; Liu, Y. T.; Lin, M. L.; He, Q.; et al. Tuning the Magnetic Properties of Self-Assembled $BiFeO_3$–$CoFe_2O_4$ Heteroepitaxy by Magneto-Structural Coupling. *Nanoscale*, **2016**, *8* (16), 8847–8854. https://doi.org/10.1039/C5NR09269H.

[20] Tian, G.; Zhang, F.; Yao, J.; Fan, H.; Li, P.; Li, Z.; Song, X.; Zhang, X.; Qin, M.; Zeng, M.; et al. Magnetoelectric Coupling in Well-Ordered Epitaxial $BiFeO_3$/$CoFe_2O_4$/$SrRuO_3$ Heterostructured Nanodot Array. *ACS Nano*, **2016**, *10* (1), 1025–1032. https://doi.org/10.1021/acsnano.5b06339.

[21] Liao, S. C.; Tsai, P. Y.; Liang, C. W.; Liu, H. J.; Yang, J. C.; Lin, S. J.; Lai, C. H.; Chu, Y. H. Misorientation Control and Functionality Design of Nanopillars in Self-Assembled Perovskite−Spinel Heteroepitaxial Nanostructures. *ACS Nano*, **2011**, *5* (5), 4118–4122. https://doi.org/10.1021/nn200880t.

[22] Li, Y.; Wang, Z.; Yao, J.; Yang, T.; Wang, Z.; Hu, J. M.; Chen, C.; Sun, R.; Tian, Z.; Li, J.; et al. Magnetoelectric Quasi-(0-3) Nanocomposite Heterostructures. *Nat Commun*, **2015**, *6* (1), 6680. https://doi.org/10.1038/ncomms7680.

[23] Yan, L.; Wang, Z.; Xing, Z.; Li, J.; Viehland, D. Magnetoelectric and Multiferroic Properties of Variously Oriented Epitaxial $BiFeO_3$–$CoFe_2O_4$ Nanostructured Thin Films. *J. Appl. Phys.*, **2010**, *107* (6), 064106. https://doi.org/10.1063/1.3359650.

[24] Zoschke, K.; Wolf, J.; Topper, M.; Ehrmann, O.; Fritzsch, T.; Scherpinski, K.; Reichl, H.; Schmuckle, F.-J. Thin Film Integration of Passives - Single Components, Filters, Integrated Passive Devices. In *2004 Proc. 54th Electronic Components and Technology Conference (IEEE Cat. No.04CH37546)*; IEEE: Las Vegas, NV, USA, 2004; pp 294–301. https://doi.org/10.1109/ECTC.2004.1319354.

[25] Dougherty, J. P.; Galvagni, J.; Marcanti, L.; Sheffield, R.; Sandborn, P.; Ulrich, R. The NEMI Roadmap: Integrated Passives Technology and Economics. **2003**, 11.

[26] Chiu, F. C.; Pan, T.-M.; Kundu, T. K.; Shih, C. H. Thin Film Applications in Advanced Electron Devices. *Adv. Mater. Sci. Eng.*, **2014**, *2014*, 1–2. https://doi.org/10.1155/2014/927358.

[27] Dix, N.; Muralidharan, R.; Rebled, J.-M.; Estradé, S.; Peiró, F.; Varela, M.; Fontcuberta, J.; Sánchez, F. Selectable Spontaneous Polarization Direction and Magnetic Anisotropy in $BiFeO_3$−$CoFe_2O_4$ Epitaxial Nanostructures. *ACS Nano*, **2010**, *4* (8), 4955–4961. https://doi.org/10.1021/nn101546r.

[28] Chen, X.; Li, X.; Shao, J.; An, N.; Tian, H.; Wang, C.; Han, T.; Wang, L.; Lu, B. High-Performance Piezoelectric Nanogenerators with Imprinted P(VDF-TrFE)/$BaTiO_3$ Nanocomposite Micropillars for Self-Powered Flexible Sensors. *Small*, **2017**, *13* (23), 1604245. https://doi.org/10.1002/smll.201604245.

[29] Zheng, H.; Zhan, Q.; Zavaliche, F.; Sherburne, M.; Straub, F.; Cruz, M. P.; Chen, L.-Q.; Dahmen, U.; Ramesh, R. Controlling Self-Assembled Perovskite−Spinel Nanostructures. *Nano Lett.*, **2006**, *6* (7), 1401–1407. https://doi.org/10.1021/nl060401y.

[30] Zheng, H.; Straub, F.; Zhan, Q.; Yang, P. L.; Hsieh, W. K.; Zavaliche, F.; Chu, Y. H.; Dahmen, U.; Ramesh, R. Self-Assembled Growth of $BiFeO_3$–$CoFe_2O_4$ Nanostructures. *Adv. Mater.*, **2006**, *18* (20), 2747–2752. https://doi.org/10.1002/adma.200601215.

[31] Amrillah, T.; Juang, J. Y. Fashioning the Architectures of the Self-Assembled Multiferroic Nanocomposite Thin Film; *AIP Conf. Proc.*, **2020**; 2314, 020012. https://doi.org/10.1063/5.0034134.

[32] Liu, H. J.; Liu, Y. Y.; Tsai, C. Y.; Liao, S. C.; Chen, Y. J.; Lin, H. J.; Lai, C. H.; Hsieh, W. F.; Li, J. Y.; Chen, C.-T.; et al. Tuning the Functionalities of a Mesocrystal via Structural Coupling. *Sci Rep*, **2015**, *5* (1), 12073. https://doi.org/10.1038/srep12073.

[33] Choi, H. K.; Aimon, N. M.; Kim, D. H.; Sun, X. Y.; Gwyther, J.; Manners, I.; Ross, C. A. Hierarchical Templating of a $BiFeO_3$–$CoFe_2O_4$ Multiferroic Nanocomposite by a Triblock Terpolymer Film. *ACS Nano*, **2014**, *8* (9), 9248–9254. https://doi.org/10.1021/nn503100s.

[34] Aimon, N. M.; Kim, D. H.; Sun, X.; Ross, C. A. Multiferroic Behavior of Templated $BiFeO_3$–$CoFe_2O_4$ Self-Assembled Nanocomposites. *ACS Appl. Mater. Interfaces*, **2015**, *7* (4), 2263–2268. https://doi.org/10.1021/am506089c.

[35] Wang, Y.; Nan, C. W. Enhanced Ferroelectricity in Ti-Doped Multiferroic $BiFeO_3$ Thin Films. *Appl. Phys. Lett.*, **2006**, *89* (5), 052903. https://doi.org/10.1063/1.2222242.

[36] Wang, Y.; Hu, J.; Lin, Y.; Nan, C. W. Multiferroic Magnetoelectric Composite Nanostructures. *NPG Asia Mater.*, **2010**, *2* (2), 61–68. https://doi.org/10.1038/asiamat.2010.32.

[37] Kim, D. H.; Aimon, N. M.; Sun, X. Y.; Kornblum, L.; Walker, Fred. J.; Ahn, Charles. H.; Ross, C. A. Integration of Self-Assembled Epitaxial $BiFeO_3$-$CoFe_2O_4$ Multiferroic Nanocomposites on Silicon Substrates. *Adv. Funct. Mater.*, **2014**, *24* (37), 5889–5896. https://doi.org/10.1002/adfm.201401458.

[38] Stern, I.; He, J.; Zhou, X.; Silwal, P.; Miao, L.; Vargas, J. M.; Spinu, L.; Kim, D. H. Role of Spinel Substrate in the Morphology of $BiFeO_3$-$CoFe_2O_4$ Epitaxial Nanocomposite Films. *Appl. Phys. Lett.*, **2011**, *99* (8), 082908. https://doi.org/10.1063/1.3631777.

[39] Zhu, Y. M.; Ke, D.; Yu, R.; Hsieh, Y. H.; Liu, H. J.; Liu, P. P.; Chu, Y. H.; Zhan, Q. Self-Assembled Perovskite-Spinel Heterostructure on a Highly Distorted Substrate. *Appl. Phys. Lett.*, **2013**, *102* (11), 111903. https://doi.org/10.1063/1.4796037.

[40] Wang, Z.; Li, Y.; Viswan, R.; Hu, B.; Harris, V. G.; Li, J.; Viehland, D. Engineered Magnetic Shape Anisotropy in $BiFeO_3$ –$CoFe_2O_4$ Self-Assembled Thin Films. *ACS Nano*, **2013**, *7* (4), 3447–3456. https://doi.org/10.1021/nn4003506.

[41] Tian, G.; Ojha, S.; Ning, S.; Gao, X.; Ross, C. A. Structure, Ferroelectricity, and Magnetism in Self-Assembled $BiFeO_3$ –$CoFe_2O_4$ Nanocomposites on (110)-$LaAlO_3$ Substrates. *Adv. Electron. Mater.*, **2019**, *5* (7), 1900012. https://doi.org/10.1002/aelm.201900012.

[42] Amrillah, T.; Quynh, L. T.; Nguyen Van, C.; Do, T. H.; Arenholz, E.; Juang, J.-Y.; Chu, Y.-H. Flexible Epsilon Iron Oxide Thin Films. *ACS Appl. Mater. Interfaces*, **2021**, acsami.0c23104. https://doi.org/10.1021/acsami.0c23104.

[43] Lee, S. H.; Tian, G.; Kim, T. C.; Jung, H. K.; Choi, J. W.; Walker, F. J.; Ahn, C. H.; Ross, C. A.; Kim, D. H. Integration of Sputter-Deposited Multiferroic $CoFe_2$

O_4–$BiFeO_3$ Nanocomposites on Conductive $La_{0.7}Sr_{0.3}MnO_3$ Electrodes. *Nanotechnology*, **2019**, *30* (10), 105601. https://doi.org/10.1088/1361-6528/aaf7cd.

[44] Kim, T. C.; Ojha, S.; Tian, G.; Lee, S. H.; Jung, H. K.; Choi, J. W.; Kornblum, L.; Walker, F. J.; Ahn, C. H.; Ross, C. A.; et al. Self-Assembled Multiferroic Epitaxial $BiFeO_3$ –$CoFe_2O_4$ Nanocomposite Thin Films Grown by RF Magnetron Sputtering. *J. Mater. Chem. C*, **2018**, *6* (20), 5552–5561. https://doi.org/10.1039/C8TC01192C.

[45] Tyagi, M.; Kumari, M.; Chatterjee, R.; Sun, A.-C.; Sharma, P. Electrical and Magnetic Properties of Multiferroic - $BiFeO_{3-x}$ $CoFe_2O_4$ Nanocomposite Thin Films Derived by Sol-gel Process. *IEEE Trans. Magn.*, 2014, *50* (1), 1–4. https://doi.org/10.1109/TMAG.2013.2278714.

[46] Xie, S.; Ma, F.; Liu, Y.; Li, J. Multiferroic $CoFe_2O_4$–$Pb(Zr_{0.52}Ti_{0.48})O_3$ Core-Shell Nanofibers and Their Magnetoelectric Coupling. *Nanoscale*, **2011**, *3* (8), 3152. https://doi.org/10.1039/c1nr10288e.

[47] Ko, K. T.; Jung, M. H.; He, Q.; Lee, J. H.; Woo, C. S.; Chu, K.; Seidel, J.; Jeon, B.-G.; Oh, Y. S.; Kim, K. H.; et al. Concurrent Transition of Ferroelectric and Magnetic Ordering near Room Temperature. *Nat Commun*, **2011**, *2* (1), 567. https://doi.org/10.1038/ncomms1576.

[48] Wang, J.; Neaton, J. B.; Zheng, H.; Nagarajan, V.; Ogale, S. B.; Liu, B.; Viehland, D.; Vaithyanathan, V.; Schlom, D. G.; Waghmare, U. V.; et al. Epitaxial $BiFeO_3$ Multiferroic Thin Film Heterostructures. *Science*, **2003**, *299* (5613), 1719-1722. https://doi.org/10.1126/science.1080615.

[49] Tahta Amrillah, Angga Hermawan, Yugandhar Bitla, Malik Anjelh Baqiya, Shu Yin, and Jenh-Yih Juang. Magnetic and Optical Properties of $CoFe_2O_4$ Mesocrystals with Different Crystal Orientations, unpublished.

[50] Palneedi, H.; Annapureddy, V.; Priya, S.; Ryu, J. Status and Perspectives of Multiferroic Magnetoelectric Composite Materials and Applications. *Actuators*, **2016**, *5* (1), 9. https://doi.org/10.3390/act5010009.

[51] Burdin, D.; Chashin, D.; Ekonomov, N.; Fetisov, L.; Fetisov, Y.; Shamonin, M. DC Magnetic Field Sensing Based on the Nonlinear Magnetoelectric Effect in Magnetic Heterostructures. *J. Phys. D: Appl. Phys.*, **2016**, *49* (37), 375002. https://doi.org/10.1088/0022-3727/49/37/375002.

[52] Fetisov, L. Y.; Serov, Vladimir. N.; Chashin, D. V.; Makovkin, S. A.; Srinivasan, G.; Viehland, D.; Fetisov, Y. K. A Magnetoelectric Sensor of Threshold DC Magnetic Fields. *J. Appl. Phys.*, **2017**, *121* (15), 154503. https://doi.org/10.1063/1.4981533.

[53] Chu, Z.; Shi, H.; PourhosseiniAsl, M. J.; Wu, J.; Shi, W.; Gao, X.; Yuan, X.; Dong, S. A Magnetoelectric Flux Gate: New Approach for Weak DC Magnetic Field Detection. *Sci. Rep.*, **2017**, *7* (1), 8592. https://doi.org/10.1038/s41598-017-09420-w.

[54] Chu, Z.; Shi, H.; Shi, W.; Liu, G.; Wu, J.; Yang, J.; Dong, S. Enhanced Resonance Magnetoelectric Coupling in (1-1) Connectivity Composites. *Adv. Mater.*, **2017**, *29* (19), 1606022. https://doi.org/10.1002/adma.201606022.

[55] Tadigadapa, S.; Mateti, K. Piezoelectric MEMS Sensors: State-of-the-Art and Perspectives. *Meas. Sci. Technol.*, **2009**, *20* (9), 092001. https://doi.org/10.1088/0957-0233/20/9/092001.

[56] Fetisov, Y. K. Piezoelectric Resonance Sensors of DC Magnetic Field. *IEEE Sensors J.*, **2014**, *14* (6), 1817–1821. https://doi.org/10.1109/JSEN.2014.2301711.

[57] Freitas, P. P.; Ferreira, R.; Cardoso, S.; Cardoso, F. Magnetoresistive Sensors. *J. Phys. Condens. Matter*, **2007**, *19* (16), 165221. https://doi.org/10.1088/0953-8984/19/16/165221.

[58] Mapps, D. J. Magnetoresistive Sensors. *Sens. Actuator A Phys.*, **1997**, *59* (1–3), 9–19. https://doi.org/10.1016/S0924-4247(97)80142-2.

[59] Mahdi, A. E.; Panina, L.; Mapps, D. Some New Horizons in Magnetic Sensing: High-Tc SQUIDs, GMR and GMI Materials. *Sens. Actuator A Phys.*, **2003**, *105* (3), 271–285. https://doi.org/10.1016/S0924-4247(03)00106-7.

[60] Primdahl, F. The Fluxgate Magnetometer. *J. Phys. E Sci. Instrum.*, **1979**, *12* (4), 241–253. https://doi.org/10.1088/0022-3735/12/4/001.

[61] Ripka, P. Advances in Fluxgate Sensors. *Sens. Actuator A Phys.*, **2003**, *106* (1–3), 8–14. https://doi.org/10.1016/S0924-4247(03)00094-3.

[62] Lu, C. C.; Huang, J.; Chiu, P. K.; Chiu, S. L.; Jeng, J. T. High-Sensitivity Low-Noise Miniature Fluxgate Magnetometers Using a Flip Chip Conceptual Design. *Sensors*, **2014**, *14* (8), 13815–13829. https://doi.org/10.3390/s140813815.

[63] Tumanski, S. Induction Coil Sensors—a Review. *Meas. Sci. Technol.*, **2007**, *18* (3), R31–R46. https://doi.org/10.1088/0957-0233/18/3/R01.

[64] Bauer, M. J.; Thomas, A.; Isenberg, B.; Varela, J.; Faria, A.; Arnold, D. P.; Andrew, J. S. Ultra-Low-Power Current Sensor Utilizing Magnetoelectric Nanowires. *IEEE Sensors J.*, **2020**, *20* (10), 5139–5145. https://doi.org/10.1109/JSEN.2020.2968224.

[65] Zhai, J.; Xing, Z.; Dong, S.; Li, J.; Viehland, D. Detection of Pico-Tesla Magnetic Fields Using Magneto-Electric Sensors at Room Temperature. *Appl. Phys. Lett.*, **2006**, *88* (6), 062510. https://doi.org/10.1063/1.2172706.

[66] Xi, H.; Qian, X.; Lu, M. C.; Mei, L.; Rupprecht, S.; Yang, Q. X.; Zhang, Q. M. A Room Temperature Ultrasensitive Magnetoelectric Susceptometer for Quantitative Tissue Iron Detection. *Sci. Rep.*, **2016**, *6* (1), 29740. https://doi.org/10.1038/srep29740.

[67] Zuo, S.; Schmalz, J.; Ozden, M. O.; Gerken, M.; Su, J.; Niekiel, F.; Lofink, F.; Nazarpour, K.; Heidari, H. Ultrasensitive Magnetoelectric Sensing System for Pico-Tesla MagnetoMyoGraphy. *IEEE Trans. Biomed. Circuits Syst.*, **2020**, *14* (5), 971–984. https://doi.org/10.1109/TBCAS.2020.2998290.

[68] Chu, Z.; Dong, C.; Tu, C.; Liang, X.; Chen, H.; Sun, C.; Yu, Z.; Dong, S.; Sun, N.-X. A Low-Power and High-Sensitivity Magnetic Field Sensor Based on Converse Magnetoelectric Effect. *Appl. Phys. Lett.*, **2019**, *115* (16), 162901. https://doi.org/10.1063/1.5122774.

[69] Hayes, P.; Jovičević Klug, M.; Toxværd, S.; Durdaut, P.; Schell, V.; Teplyuk, A.; Burdin, D.; Winkler, A.; Weser, R.; Fetisov, Y.; et al. Converse Magnetoelectric Composite Resonator for Sensing Small Magnetic Fields. *Sci. Rep.*, **2019**, *9* (1), 16355. https://doi.org/10.1038/s41598-019-52657-w.

[70] Fetisov, Y. K.; Burdin, D. A.; Chashin, D. V.; Ekonomov, N. A. High-Sensitivity Wideband Magnetic Field Sensor Using Nonlinear Resonance Magnetoelectric Effect. *IEEE Sensors J.*, **2014**, *14* (7), 2252–2256. https://doi.org/10.1109/JSEN.2014.2309718.

[71] Zhuang, X.; Lam Chok Sing, M.; Dolabdjian, C. Investigation of the Near-Carrier Noise for Strain-Driven ME Laminates by Using Cross-Correlation Techniques. *IEEE Trans. Magn.*, **2013**, *49* (1), 120–123. https://doi.org/10.1109/TMAG.2012.2220340.

[72] Wang, Y. J.; Gao, J. Q.; Li, M. H.; Shen, Y.; Hasanyan, D.; Li, J. F.; Viehland, D. A Review on Equivalent Magnetic Noise of Magnetoelectric Laminate Sensors.

Phil. Trans. R. Soc. A., **2014**, *372* (2009), 20120455. https://doi.org/10.1098/rsta.2012.0455.

[73] Bauer, M. J. Magnetic Field Sensors Using Arrays of Electrospun Magnetoelectric Janus Nanowires. *Microsyst. Nanoeng.*, **2018**, 4 (37), 1-12.

[74] Radchenko, G. S.; Radchenko, M. G. Magnet-Metal-Piezoelectric Magnetic Sensor with the Highest Magnetoelectric Coefficient. *Tech. Phys.*, **2014**, *59* (10), 1457–1461. https://doi.org/10.1134/S1063784214100259.

[75] Bhatti, S.; Sbiaa, R.; Hirohata, A.; Ohno, H.; Fukami, S.; Piramanayagam, S. N. Spintronics Based Random Access Memory: A Review. *Mater. Today*, **2017**, *20* (9), 530–548. https://doi.org/10.1016/j.mattod.2017.07.007.

[76] Grollier, J.; Querlioz, D.; Camsari, K. Y.; Everschor-Sitte, K.; Fukami, S.; Stiles, M. D. Neuromorphic Spintronics. *Nat. Electron.*, **2020**, *3* (7), 360–370. https://doi.org/10.1038/s41928-019-0360-9.

[77] Salahuddin, S.; Ni, K.; Datta, S. The Era of Hyper-Scaling in Electronics. *Nat Electron*, **2018**, *1* (8), 442–450. https://doi.org/10.1038/s41928-018-0117-x.

[78] Li, X.; Lee, A.; Razavi, S. A.; Wu, H.; Wang, K. L. Voltage-Controlled Magnetoelectric Memory and Logic Devices. *MRS Bull.*, **2018**, *43* (12), 970–977. https://doi.org/10.1557/mrs.2018.298.

[79] Wang, K. L.; Lee, H.; Khalili Amiri, P. Magnetoelectric Random Access Memory-Based Circuit Design by Using Voltage-Controlled Magnetic Anisotropy in Magnetic Tunnel Junctions. *IEEE Trans. Nanotechnol.*, **2015**, *14* (6), 992–997. https://doi.org/10.1109/TNANO.2015.2462337.

[80] Meena, J.; Sze, S.; Chand, U.; Tseng, T. Y. Overview of Emerging Nonvolatile Memory Technologies. *Nanoscale Res. Lett.*, **2014**, *9* (1), 526. https://doi.org/10.1186/1556-276X-9-526.

[81] Shen, J.; Cong, J.; Shang, D.; Chai, Y.; Shen, S.; Zhai, K.; Sun, Y. A Multilevel Nonvolatile Magnetoelectric Memory. *Sci. Rep.*, **2016**, *6* (1), 34473. https://doi.org/10.1038/srep34473.

[82] Kosub, T.; Kopte, M.; Hühne, R.; Appel, P.; Shields, B.; Maletinsky, P.; Hübner, R.; Liedke, M. O.; Fassbender, J.; Schmidt, O. G.; et al. Purely Antiferromagnetic Magnetoelectric Random Access Memory. *Nat. Commun.*, **2017**, *8* (1), 13985. https://doi.org/10.1038/ncomms13985.

[83] Bibes, M.; Barthélémy, A. Towards a Magnetoelectric Memory. *Nat. Mater.*, **2008**, *7* (6), 425–426. https://doi.org/10.1038/nmat2189.

[84] Chu, Y. H.; Martin, L. W.; Holcomb, M. B.; Gajek, M.; Han, S. J.; He, Q.; Balke, N.; Yang, C. H.; Lee, D.; Hu, W.; et al. Electric-Field Control of Local Ferromagnetism Using a Magnetoelectric Multiferroic. *Nat. Mater.*, **2008**, *7* (6), 478–482. https://doi.org/10.1038/nmat2184.

[85] Chen, X.; Hochstrat, A.; Borisov, P.; Kleemann, W. Magnetoelectric Exchange Bias Systems in Spintronics. *Appl. Phys. Lett.*, **2006**, *89* (20), 202508. https://doi.org/10.1063/1.2388149.

[86] Sbiaa, R.; Piramanayagam, S. N. Recent Developments in Spin Transfer Torque MRAM. *Phys. Status Solidi RRL*, **2017**, *11* (12), 1700163. https://doi.org/10.1002/pssr.201700163.

[87] Albrecht, T. R.; Arora, H.; Ayanoor-Vitikkate, V.; Beaujour, J.-M.; Bedau, D.; Berman, D.; Bogdanov, A. L.; Chapuis, Y.-A.; Cushen, J.; Dobisz, E. E.; et al. Bit-Patterned Magnetic Recording: Theory, Media Fabrication, and Recording Performance. *IEEE Trans. Magn.*, **2015**, *51* (5), 1–42. https://doi.org/10.1109/TMAG.2015.2397880.

[88] Richter, H. J.; Dobin, A. Y.; Heinonen, O.; Gao, K. Z.; v.d. Veerdonk, R. J. M.; Lynch, R. T.; Xue, J.; Weller, D.; Asselin, P.; Erden, M. F.; et al. Recording on Bit-Patterned Media at Densities of 1 Tb/In^2 and Beyond. *IEEE Trans. Magn.*, **2006**, *42* (10), 2255–2260. https://doi.org/10.1109/TMAG.2006.878392.

[89] Kikitsu, A. Prospects for Bit Patterned Media for High-Density Magnetic Recording. *J. Magn. Magn. Mater.*, **2009**, *321* (6), 526–530. https://doi.org/10.1016/j.jmmm.2008.05.039.

[90] Yu, Y.; Xu, F.; Wang, N.; Zou, L.; Xue, F. Dynamic Cantilever Magnetometry of Individual Co Nanosheets and Applicable Conditions of Uniaxial Magnetic Anisotropy Assumption. *Jpn. J. Appl. Phys.*, **2018**, *57* (9), 090312. https://doi.org/10.7567/JJAP.57.090312.

[91] Yanagihara, H.; Uwabo, K.; Minagawa, M.; Kita, E.; Hirota, N. Perpendicular Magnetic Anisotropy in $CoFe_2O_4$ (001) Films Epitaxially Grown on MgO(001). *J. Appl. Phys.*, **2011**, *109* (7), 07C122. https://doi.org/10.1063/1.3566079.

[92] Thang, P. D.; Rijnders, G.; Blank, D. H. A. Stress-Induced Magnetic Anisotropy of $CoFe_2O_4$ Thin Films Using Pulsed Laser Deposition. *J. Magn. Magn. Mater.*, **2007**, *310* (2), 2621–2623. https://doi.org/10.1016/j.jmmm.2006.11.048.

[93] Park, S. Y.; Kim, D. S.; Liu, Y.; Hwang, J.; Kim, Y.; Kim, W.; Kim, J.-Y.; Petrovic, C.; Hwang, C.; Mo, S.-K.; et al. Controlling the Magnetic Anisotropy of

the van Der Waals Ferromagnet Fe_3GeTe_2 through Hole Doping. *Nano Lett.*, **2020**, *20* (1), 95–100. https://doi.org/10.1021/acs.nanolett.9b03316.

[94] Larson, P.; Mazin, I. I.; Papaconstantopoulos, D. A. Effects of Doping on the Magnetic Anisotropy Energy in $SmCo_{5-x}Fe_x$ and $YCo_{5-x}Fe_x$. *Phys. Rev. B*, **2004**, *69* (13), 134408. https://doi.org/10.1103/PhysRevB.69.134408.

[95] Iida, Y.; Xiang, Q.; Okabayashi, J.; Scheike, T.; Sukegawa, H.; Mitani, S. Effect of Tungsten Doping on Perpendicular Magnetic Anisotropy and Its Voltage Effect in Single Crystal Fe/MgO(001) Interfaces. *J. Phys. D Appl. Phys.*, **2020**, *53* (12), 124001. https://doi.org/10.1088/1361-6463/ab5c93.

[96] Bao, Z.; Chen, X. Flexible and Stretchable Devices. *Adv. Mater.*, **2016**, *28* (22), 4177–4179. https://doi.org/10.1002/adma.201601422.

[97] Liu, W.; Wang, H. Flexible Oxide Epitaxial Thin Films for Wearable Electronics: Fabrication, Physical Properties, and Applications. *J. Materiomics*, **2020**, *6* (2), 385–396. https://doi.org/10.1016/j.jmat.2019.12.006.

[98] Zou, M.; Ma, Y.; Yuan, X.; Hu, Y.; Liu, J.; Jin, Z. Flexible Devices: From Materials, Architectures to Applications. *J. Semicond.*, **2018**, *39* (1), 011010. https://doi.org/10.1088/1674-4926/39/1/011010.

[99] Sun, B.; Long, Y. Z.; Chen, Z. J.; Liu, S. L.; Zhang, H. D.; Zhang, J. C.; Han, W. P. Recent Advances in Flexible and Stretchable Electronic Devices via Electrospinning. *J. Mater. Chem. C*, **2014**, *2* (7), 1209–1219. https://doi.org/10.1039/C3TC31680G.

[100] Nathan, A.; Ahnood, A.; Cole, M. T.; Sungsik Lee; Suzuki, Y.; Hiralal, P.; Bonaccorso, F.; Hasan, T.; Garcia-Gancedo, L.; Dyadyusha, A.; et al. Flexible Electronics: The Next Ubiquitous Platform. *Proc. IEEE*, **2012**, *100* (Special Centennial Issue), 1486–1517. https://doi.org/10.1109/JPROC.2012.2190168.

[101] Huang, S.; Liu, Y.; Zhao, Y.; Ren, Z.; Guo, C. F. Flexible Electronics: Stretchable Electrodes and Their Future. *Adv. Funct. Mater.*, **2019**, *29* (6), 1805924. https://doi.org/10.1002/adfm.201805924.

[102] Bitla, Y.; Chu, Y. H. MICAtronics: A New Platform for Flexible X-Tronics. *FlatChem*, **2017**, *3*, 26–42. https://doi.org/10.1016/j.flatc.2017.06.003.

[103] Wu, P. C.; Chu, Y. H. Development of Oxide Heteroepitaxy for Soft Technology. *J. Mater. Chem. C*, **2018**, *6* (23), 6102–6117. https://doi.org/10.1039/C8TC00959G.

[104] Liu, H. J.; Wang, C. K.; Su, D.; Amrillah, T.; Hsieh, Y. H.; Wu, K. H.; Chen, Y. C.; Juang, J. Y.; Eng, L. M.; Jen, S. U.; et al. Flexible Heteroepitaxy of $CoFe_2O_4$/Muscovite Bimorph with Large Magnetostriction. *ACS Appl. Mater. Interfaces*, **2017**, *9* (8), 7297–7304. https://doi.org/10.1021/acsami.6b16485.

[105] Annapureddy, V.; Palneedi, H.; Hwang, G. T.; Peddigari, M.; Jeong, D. Y.; Yoon, W. H.; Kim, K. H.; Ryu, J. Magnetic Energy Harvesting with Magnetoelectrics: An Emerging Technology for Self-Powered Autonomous Systems. *Sustain. Energy Fuels*, **2017**, *1* (10), 2039–2052. https://doi.org/10.1039/C7SE00403F.

[106] Sriramdas, R.; Kang, M.; Meng, M.; Kiani, M.; Ryu, J.; Sanghadasa, M.; Priya, S. Large Power Amplification in Magneto-Mechano-Electric Harvesters through Distributed Forcing. *Adv. Energy Mater.*, **2020**, *10* (8), 1903689. https://doi.org/10.1002/aenm.201903689.

[107] Yan, L.; Zhuo, M.; Wang, Z.; Yao, J.; Haberkorn, N.; Zhang, S.; Civale, L.; Li, J.; Viehland, D.; Jia, Q. X. Magnetoelectric Properties of Flexible $BiFeO_3$/Ni Tapes. *Appl. Phys. Lett.*, **2012**, *101* (1), 012908. https://doi.org/10.1063/1.4731780.

[108] Wang, Z.; Yan, L.; Yang, Y.; Li, J. F.; Das, J.; Geiler, A. L.; Yang, A.; Chen, Y.; Harris, V. G.; Viehland, D. Magnetoelectric Effect in Crystallographically Textured BaTiO3 Films Deposited on Ferromagnetic Metallic Glass Foils. *J. Appl. Phys.*, **2011**, *109* (3), 034102. https://doi.org/10.1063/1.3544352.

[109] Shin, S. H.; Choi, S. Y.; Lee, M. H.; Nah, J. High-Performance Piezoelectric Nanogenerators via Imprinted Sol–Gel $BaTiO_3$ Nanopillar Array. *ACS Appl. Mater. Interfaces*, **2017**, *9* (47), 41099–41103. https://doi.org/10.1021/acsami.7b11773.

[110] Zhang, Y.; Ma, C.; Lu, X.; Liu, M. Recent Progress on Flexible Inorganic Single-Crystalline Functional Oxide Films for Advanced Electronics. *Mater. Horiz.*, **2019**, *6* (5), 911–930. https://doi.org/10.1039/C8MH01598H.

[111] Furukawa, T.; Seo, N. Electrostriction as the Origin of Piezoelectricity in Ferroelectric Polymers. *Jpn. J. Appl. Phys.*, **1990**, *29* (Part 1, No. 4), 675–680. https://doi.org/10.1143/JJAP.29.675.

[112] Wang, A. C.; Wu, C.; Pisignano, D.; Wang, Z. L.; Persano, L. Polymer Nanogenerators: Opportunities and Challenges for Large-scale Applications. *J. Appl. Polym. Sci.*, **2018**, *135* (24), 45674. https://doi.org/10.1002/app.45674.

[113] Li, J. F.; Dai, X.; Chow, A.; Viehland, D. Polarization Switching Mechanisms and Electromechanical Properties of La-Modified Lead Zirconate Titanate Ceramics. *J. Mater. Res.*, **1995**, *10* (4), 926–938. https://doi.org/10.1557/JMR.1995.0926.

[114] Mettout, B.; Gisse, P. Theory of the Photovoltaic and Photo-Magneto-Electric Effects in Multiferroic Materials. *Ferroelectrics*, **2017**, *506* (1), 93–110. https://doi.org/10.1080/00150193.2017.1282263.

[115] Biswas, P. P.; Chinthakuntla, T.; Duraisamy, D.; Nambi Venkatesan, G.; Venkatachalam, S.; Murugavel, P. Photovoltaic and Photo-Capacitance Effects in Ferroelectric $BiFeO_3$ Thin Film. *Appl. Phys. Lett.*, **2017**, *110* (19), 192906. https://doi.org/10.1063/1.4983378.

[116] Singh, S.; Khare, N. Low Field Magneto-Tunable Photocurrent in $CoFe_2O_4$ Nanostructure Films for Enhanced Photoelectrochemical Properties. *Sci. Rep.*, **2018**, *8* (1), 6522. https://doi.org/10.1038/s41598-018-24947-2.

[117] Muhammad, A.; Sato-Turtelli, R.; Kriegisch, M.; Grössinger, R.; Kubel, F.; Konegger, T. Large Enhancement of Magnetostriction Due to Compaction Hydrostatic Pressure and Magnetic Annealing in $CoFe_2O_4$. *J. Appl. Phys.*, **2012**, *111* (1), 013918. https://doi.org/10.1063/1.3675489.

[118] Hou, Y. H.; Zhao, Y. J.; Liu, Z. W.; Yu, H. Y.; Zhong, X. C.; Qiu, W. Q.; Zeng, D. C.; Wen, L. S. Structural, Electronic and Magnetic Properties of Partially Inverse Spinel $CoFe_2O_4$: A First-Principles Study. *J. Phys. D Appl. Phys.*, **2010**, *43* (44), 445003. https://doi.org/10.1088/0022-3727/43/44/445003.

[119] Nlebedim, I. C.; Melikhov, Y.; Jiles, D. C. Temperature Dependence of Magnetic Properties of Heat Treated Cobalt Ferrite. *J. Appl. Phys.*, **2014**, *115* (4), 043903. https://doi.org/10.1063/1.4862300.

[120] Ravindra, A. V.; Padhan, P.; Prellier, W. Electronic Structure and Optical Band Gap of $CoFe_2O_4$ Thin Films. *Appl. Phys. Lett.*, **2012**, *101* (16), 161902. https://doi.org/10.1063/1.4759001.

[121] Rai, R. C.; Wilser, S.; Guminiak, M.; Cai, B.; Nakarmi, M. L. Optical and Electronic Properties of $NiFe_2O_4$ and $CoFe_2O_4$ Thin Films. *Appl. Phys. A*, **2012**, *106* (1), 207–211. https://doi.org/10.1007/s00339-011-6549-z.

[122] Pan, D. F.; Chen, G. Y.; Bi, G. F.; Zhang, H.; Liu, J. M.; Wang, G. H.; Wan, J. G. Tuning the Photovoltaic Effect of Multiferroic $CoFe_2O_4$/$Pb(Zr,Ti)O_3$ Composite

Films by Magnetic Fields. *Appl. Phys. Lett.*, **2016**, *108* (22), 222902. https://doi.org/10.1063/1.4953154.

[123] Quynh, L. T.; Van, C. N.; Bitla, Y.; Chen, J.-W.; Do, T. H.; Tzeng, W. Y.; Liao, S. C.; Tsai, K. A.; Chen, Y. C.; Wu, C. L.; et al. Self-Assembled $BiFeO_3$-ε-Fe_2O_3 Vertical Heteroepitaxy for Visible Light Photoelectrochemistry. *Adv. Energy Mater.*, **2016**, *6* (18), 1600686. https://doi.org/10.1002/aenm.201600686.

[124] Sonu; Dutta, V.; Sharma, S.; Raizada, P.; Hosseini-Bandegharaei, A.; Kumar Gupta, V.; Singh, P. Review on Augmentation in Photocatalytic Activity of $CoFe_2O_4$ via Heterojunction Formation for Photocatalysis of Organic Pollutants in Water. *J. Saudi Chem. Society*, **2019**, *23* (8), 1119–1136. https://doi.org/10.1016/j.jscs.2019.07.003.

[125] Cao, Z.; Zuo, C. Direct Synthesis of Magnetic $CoFe_2O_4$ Nanoparticles as Recyclable Photo-Fenton Catalysts for Removing Organic Dyes. *ACS Omega*, **2020**, *5* (35), 22614–22620. https://doi.org/10.1021/acsomega.0c03404.

[126] Kim, C. W.; Yeob, S. J.; Cheng, H.-M.; Kang, Y. S. A Selectively Exposed Crystal Facet-Engineered TiO_2 Thin Film Photoanode for the Higher Performance of the Photoelectrochemical Water Splitting Reaction. *Energy Environ. Sci.*, **2015**, *8* (12), 3646–3653. https://doi.org/10.1039/C5EE02300A.

[127] Nalajala, N.; Patra, K. K.; Bharad, P. A.; Gopinath, C. S. Why the Thin Film Form of a Photocatalyst Is Better than the Particulate Form for Direct Solar-to-Hydrogen Conversion: A Poor Man's Approach. *RSC Adv.*, **2019**, *9* (11), 6094–6100. https://doi.org/10.1039/C8RA09982K.

[128] Wang, H.; Zhang, H.; Wang, Z.; Xia, X.; Bao, Y.; Homewood, K.; d' Assunção Lourenço, M.; Shao, G.; Gao, Y. In-Situ Hydrogen Production and Storage in (002) Oriented TiO_2 Thin Films. *Appl. Surf. Sci.*, **2020**, *509*, 145366. https://doi.org/10.1016/j.apsusc.2020.145366.

[129] Khodadadian, F.; de la Garza, F. G.; van Ommen, J. R.; Stankiewicz, A. I.; Lakerveld, R. The Application of Automated Feedback and Feedforward Control to a LED-Based Photocatalytic Reactor. *Chem. Eng. J.*, **2019**, *362*, 375–382. https://doi.org/10.1016/j.cej.2018.12.134.

[130] Zhang, Y.; Liang, C.; Wu, J.; Liu, H.; Zhang, B.; Jiang, Z.; Li, S.; Xu, P. Recent Advances in Magnetic Field-Enhanced Electrocatalysis. *ACS Appl. Energy Mater.*, **2020**, *3* (11), 10303–10316. https://doi.org/10.1021/acsaem.0c02104.

[131] Chen, X. Y.; Yu, T.; Gao, F.; Zhang, H. T.; Liu, L. F.; Wang, Y. M.; Li, Z. S.; Zou, Z. G.; Liu, J. M. Application of Weak Ferromagnetic $BiFeO_3$ Films as the Photoelectrode Material under Visible-Light Irradiation. *Appl. Phys. Lett.*, **2007**, *91* (2), 022114. https://doi.org/10.1063/1.2757132.

[132] Ji, W.; Yao, K.; Lim, Y. F.; Liang, Y. C.; Suwardi, A. Epitaxial Ferroelectric $BiFeO_3$ Thin Films for Unassisted Photocatalytic Water Splitting. *Appl. Phys. Lett.*, **2013**, *103* (6), 062901. https://doi.org/10.1063/1.4817907.

[133] Song, J.; Kim, T. L.; Lee, J.; Cho, S. Y.; Cha, J.; Jeong, S. Y.; An, H.; Kim, W. S.; Jung, Y.-S.; Park, J.; et al. Domain-Engineered $BiFeO_3$ Thin-Film Photoanodes for Highly Enhanced Ferroelectric Solar Water Splitting. *Nano Res.*, **2018**, *11* (2), 642–655. https://doi.org/10.1007/s12274-017-1669-1.

[134] Liu, G.; Karuturi, S. K.; Chen, H.; Wang, D.; Ager, J. W.; Simonov, A. N.; Tricoli, A. Enhancement of the Photoelectrochemical Water Splitting by Perovskite $BiFeO_3$ via Interfacial Engineering. *Solar Energy*, **2020**, *202*, 198–203. https://doi.org/10.1016/j.solener.2020.03.117.

[135] Li, C.; Baek, J. B. Recent Advances in Noble Metal (Pt, Ru, and Ir)-Based Electrocatalysts for Efficient Hydrogen Evolution Reaction. *ACS Omega*, **2020**, *5* (1), 31–40. https://doi.org/10.1021/acsomega.9b03550.

[136] Shao, M.; Shoemaker, K.; Peles, A.; Kaneko, K.; Protsailo, L. Pt Monolayer on Porous Pd−Cu Alloys as Oxygen Reduction Electrocatalysts. *J. Am. Chem. Soc.*, **2010**, *132* (27), 9253–9255. https://doi.org/10.1021/ja101966a.

[137] Gu, H.; Yang, Y.; Tian, J.; Shi, G. Photochemical Synthesis of Noble Metal (Ag, Pd, Au, Pt) on Graphene/ZnO Multihybrid Nanoarchitectures as Electrocatalysis for H_2O_2 Reduction. *ACS Appl. Mater. Interfaces*, **2013**, *5* (14), 6762–6768. https://doi.org/10.1021/am401738k.

[138] Huang, Y.; Yang, W.; Yu, Y.; Hao, S. Ordered Mesoporous Spinel $CoFe_2O_4$ as Efficient Electrocatalyst for the Oxygen Evolution Reaction. *J. Electroanal. Chem.*, **2019**, *840*, 409–414. https://doi.org/10.1016/j.jelechem.2019.04.010.

[139] Si, C.; Zhang, Y.; Zhang, C.; Gao, H.; Ma, W.; Lv, L.; Zhang, Z. Mesoporous Nanostructured Spinel-Type MFe_2O_4 (M = Co, Mn, Ni) Oxides as Efficient Bi-Functional Electrocatalysts towards Oxygen Reduction and Oxygen Evolution. *Electrochim. Acta*, **2017**, *245*, 829–838. https://doi.org/10.1016/j.electacta.2017.06.029.

[140] Yan, W.; Bian, W.; Jin, C.; Tian, J.-H.; Yang, R. An Efficient Bi-Functional Electrocatalyst Based on Strongly Coupled $CoFe_2O_4$/Carbon Nanotubes Hybrid for Oxygen Reduction and Oxygen Evolution. *Electrochim. Acta*, **2015**, *177*, 65–72. https://doi.org/10.1016/j.electacta.2015.02.044.

[141] Liu, S.; Bian, W.; Yang, Z.; Tian, J.; Jin, C.; Shen, M.; Zhou, Z.; Yang, R. A Facile Synthesis of $CoFe_2O_4$/Biocarbon Nanocomposites as Efficient Bi-Functional Electrocatalysts for the Oxygen Reduction and Oxygen Evolution Reaction. *J. Mater. Chem. A*, **2014**, *2* (42), 18012–18017. https://doi.org/10.1039/C4TA04115A.

[142] Nodo, S.; Yamamoto, T.; Yanase, T.; Shimada, T.; Nagahama, T. Characterization of Magnetic Properties of Ultrathin $CoFe_2O_4$ Films by Utilizing Magnetic Proximity Effect. *Solid State Commun.*, **2020**, *306*, 113762. https://doi.org/10.1016/j.ssc.2019.113762.

[143] Hossain, A.; Sarker, M. S. I.; Khan, M. K. R.; Rahman, M. M. Spin Effect on Electronic, Magnetic and Optical Properties of Spinel $CoFe_2O_4$: A DFT Study. *Mater. Sci. Eng. B*, **2020**, *253*, 114496. https://doi.org/10.1016/j.mseb.2020.114496.

[144] Elias, L.; Chitharanjan Hegde, A. Effect of Magnetic Field on HER of Water Electrolysis on Ni–W Alloy. *Electrocatalysis*, **2017**, *8* (4), 375–382. https://doi.org/10.1007/s12678-017-0382-x.

[145] Niether, C.; Faure, S.; Bordet, A.; Deseure, J.; Chatenet, M.; Carrey, J.; Chaudret, B.; Rouet, A. Improved Water Electrolysis Using Magnetic Heating of FeC–Ni Core–Shell Nanoparticles. *Nat. Energy.*, **2018**, *3* (6), 476–483. https://doi.org/10.1038/s41560-018-0132-1.

[146] Monica Chhabra; Asavari Patil; Vineet Kumar. Magnetic Sensor Market Outlook - 2026. https://www.alliedmarketresearch.com/magnetic-sensor-market (accessed November 20, 2020).

[147] Sikder, A. K.; Petracca, G.; Aksu, H.; Jaeger, T.; Uluagac, A. S. A Survey on Sensor-Based Threats to Internet-of-Things (IoT) Devices and Applications. *arXiv:1802.02041 [cs]*, **2018**.

[148] Liu, X.; Lam, K. H.; Zhu, K.; Zheng, C.; Li, X.; Du, Y.; Liu, C.; Pong, P. W. T. Overview of Spintronic Sensors, Internet of Things, and Smart Living. *arXiv:1611.00317 [cs]*, **2016**.

[149] Mori, T.; Priya, S. Materials for Energy Harvesting: At the Forefront of a New Wave. *MRS Bull.*, **2018**, *43* (3), 176–180. https://doi.org/10.1557/mrs.2018.32.

[150] Laurent Probst; Bertrand Pedersen; Lauriane Dakkak-Arnoux. Energy harvesting to power the rise of the Internet of Things. https://ec.europa.eu/growth/tools-databases/dem/monitor/sites/default/files/DTM_Energy%20harvesting%20v1_0.pdf (accessed November 20, 2020).

[151] Elahi, H.; Munir, K.; Eugeni, M.; Atek, S.; Gaudenzi, P. Energy Harvesting towards Self-Powered IoT Devices. *Energies*, **2020**, *13* (21), 5528. https://doi.org/10.3390/en13215528.

[152] Mufti, N.; Amrillah, T.; Taufiq, A.; Sunaryono; Aripriharta; Diantoro, M.; Zulhadjri; Nur, H. Review of CIGS-Based Solar Cells Manufacturing by Structural Engineering. *Solar Energy*, **2020**, *207*, 1146–1157. https://doi.org/10.1016/j.solener.2020.07.065.

[153] Zhou, H.; Chen, Q.; Li, G.; Luo, S.; Song, T. b.; Duan, H. S.; Hong, Z.; You, J.; Liu, Y.; Yang, Y. Interface Engineering of Highly Efficient Perovskite Solar Cells. *Science*, **2014**, *345* (6196), 542–546. https://doi.org/10.1126/science.1254050.

[154] O'Dea. S. Smartphone users worldwide 2016-2021. https://www.statista.com/statistics/330695/number-of-smartphone-users-worldwide/ (accessed November 20, 2020).

[155] marketsandmarkets. smart homes market reports. https://www.marketsandmarkets.com/Market-Reports/smart-homes-and-assisted-living- advanced-technologie-and-global-market-121.html (accessed November 20, 2020).

[156] Sönnichsen. Worldwide demand for solar photovoltaics outlook 2015-2024. https://www.statista.com/statistics/500250/solar-photovoltaic-demand-outlook-worldwide/ (accessed November 21, 2020).

[157] Hariharan. S; Prasad. E. Solar Energy Market Outlook – 2026. https://www.alliedmarketresearch.com/solar-energy-market (accessed November 21, 2020).

[158] Valuates Reports. IoT Device Management Market Size USD 6254.6 Million by 2026 at CAGR 22.6%. https://www.prnewswire.com/news-releases/iot-device-management-market-size-usd-6254-6-million-by-2026-at-cagr-22-6--valuates-reports-

301186507.html#:~:text=Internet%20of%20Things%20(IoT)%20Market,38.62%25%20between%202018%20and%202025.&text=IoT%20Devices%20and%20Sensors%20Market,Market%20Research%20Report%202020%2D2026 (accessed November 21, 2020).

[159] Persistence market research. Global Market Study on Photocatalyst: Increasing Applicability in Air Purification Favoring Demand Growth. https://www.persistencemarketresearch.com/market-research/photocatalysts-market.asp (accessed November 21, 2020).

[160] Staedler, D.; Passemard, S.; Magouroux, T.; Rogov, A.; Maguire, C. M.; Mohamed, B. M.; Schwung, S.; Rytz, D.; Jüstel, T.; Hwu, S.; et al. Cellular Uptake and Biocompatibility of Bismuth Ferrite Harmonic Advanced Nanoparticles. *Nanomedicine: Nanotechnology, Biology and Medicine*, **2015**, *11* (4), 815–824. https://doi.org/10.1016/j.nano.2014.12.018.

[161] Velho-Pereira, S.; Noronha, A.; Mathias, A.; Zakane, R.; Naik, V.; Naik, P.; Salker, A. V.; Naik, S. R. Antibacterial Action of Doped $CoFe_2O_4$ Nanocrystals on Multidrug Resistant Bacterial Strains. *Materials Science and Engineering: C*, **2015**, *52*, 282–287. https://doi.org/10.1016/j.msec.2015.03.046.

[162] Jaffari, Z. H.; Lam, S.-M.; Sin, J.-C.; Zeng, H.; Mohamed, A. R. Magnetically Recoverable Pd-Loaded $BiFeO_3$ Microcomposite with Enhanced Visible Light Photocatalytic Performance for Pollutant, Bacterial and Fungal Elimination. *Separation and Purification Technology*, **2020**, *236*, 116195. https://doi.org/10.1016/j.seppur.2019.116195.

Table 1. Recent fabrications and possible applications of BFO-CFO nanocomposite thin-film

Fabrications Methods	Substrate and Architecture Design	Magnetic or Electric or Magnetoelectric Coefficient
PLD	STO-(100) (1-3 system)[8]	α_{ME} = 60 mV/cm.Oe[8]
PLD	STO-(110) (1-3 system)[23]	α_{ME} = 15 mV/cm.Oe[23]
PLD	STO-(111) (1-3 system)[23]	α_{ME} = 8 mV/cm.Oe[23]
PLD	Mica-(100) (1-3 system)[9]	α_{ME} = 74 mV/cm.Oe, d_{33} = 76.5 pm/V, M_s = ~220 emu/cm^3[9]
PLD	STO-(100) (Quasi 0-3 system)[22]	α_{ME} = 338 mV/cm.Oe[22] (microscopic magnetoelectric measurement)
PLD	STO-(100) (well-ordered nanodot array)[20]	α_{ME} = 18000 mV/cm.Oe[20] (microscopic magnetoelectric measurement)
PLD	NSTO-(100) (well-ordered 1-3 system)[33]	M_s = 85 emu/cm^3, $H_{k,me}$ = 7 kOe[33]
PLD	LAO-(100) (1-3 system)[19]	M_s = ~200 emu/cm^3, H_c = 2.5 kOe[19]
PLD	LAO (110) (1-3 system)[41]	M_s = 70 emu/cm^3, M_r = 20 emu/cm^3, H_c = 600 Oe[41]
PLD	DSO (110) (1-3 system)[21]	-
PLD	NGO (110) (1-3 system)[21]	-
PLD	MAO (100) (1-3 system)[27, 38]	M_s = 430 emu/cm^3, $H_{ans.}$ = 35 kOe[38]
PLD	MgO (100) (1-3 system)[27]	-
PLD	Si (100) (1-3 system)[37]	M_s = ~70 emu/cm^3, H_c = 12 – 13 kOe[37]
PED	NSTO-(100) (well-ordered 1-3 system)[18]	d_{33} = 5 – 10 pm/V[18]
Sputtering	STO-(100) (1-3 system)[43]	H_{me} = 20.3 kOe, M_s = ~70 emu/cm^3[43]

RF Magnetron sputtering	Si (001) (1-3 system)[44]	H_{me} = 23.0 kOe, M_s = ~70 emu/cm^3, M_r = ~45 emu/cm^3, H_c = ~4000 Oe[44]
Sol-gel and spin-coating	ITO glass (textured thin-film)[45]	M_s = 196 emu/cm^3, H_c = 1.21 kOe, P_r = 10 μC/cm^2[45]
Applications	Advantage	Disadvantage
Magnetic Sensor	- The magnetoelectric based magnetic sensors are possible to replace the Hall sensors which largely used nowadays due to ultra-low power consumption operation - BFO-CFO could suitable for DC magnetic-field measurement from nano- to mili-tesla. Therefore, BFO-CFO possible to sense the biomagnetic signal	- Compilated fabrication process compared to the bilayer magnetoelectric thin-film
Memory Devices	- Magnetoelectric coupling in BFO-CFO could generate energy-efficient of memory devices - Could be used as BPM application with high density due to scalable size of isolated nanomagnetic CFO	- Magnetic anisotropy is smaller than metal alloy such as CoFeB that recently used for nonvolatile memory
Energy harvesting devices	- Strong magnetoelectric coupling in flexible BFO-CFO VAN could induce an electrical charge when stressed even by a negligibly low magnetic field, therefore only need low-frequency magnetic	- Complicated fabrication considering crystallinity of BFO-CFO VAN - Difficulties of BFO-CFO VAN having VAN structure grown on large scale flexible substrate.

	fields to generate power thus can be employed as wireless power transfer for operating IoT devices	
Photovoltaic devices	- Electric polarization can enhance the photovoltaic effect, while ferroelectric domains can separate the photon-generated charge carriers - Appropriate candidate to obtain hybrid materials having ability tunable photovoltaic with the magnetic field	- BFO-CFO VAN has a smaller light absorption ability compared to the well-known photovoltaic thin-film system such as CIGS or silicon tandem solar cell. - BFO-CFO VAN thin-film is difficult to fabricate in a large-scale area
Magneto-photocatalyst devices	- Magnetoelectric BFO-CFO nanocomposite capable of initiating an electrochemical process under the application of alternating magnetic fields - The design of photocatalytic thin-films would be ideal industrial scale - The catalysts activity of thin-film is obtained outperformed the particulate - Photocatalysts thin-film lead to cost-effective hydrogen production	- BFO-CFO VAN thin-film is difficult to fabricate in a large-scale area
Magnetic field-induced electrocatalyst device	- Combination of high spin polarization of CFO and strong spontaneous electrical polarization of BFO can	- Need special electrolyzer designs for the convenient exploitation

	improve the electrocatalysis hydrogen and oxygen reaction	

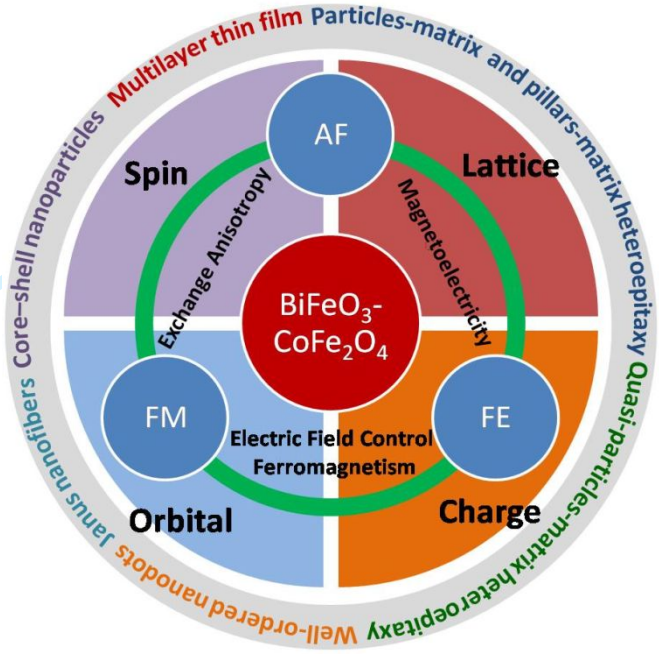

Figure 1. The combination of multiferroic BFO and ferromagnetic CFO obtained in various forms yields an extension property and excellent magnetoelectric coupling.

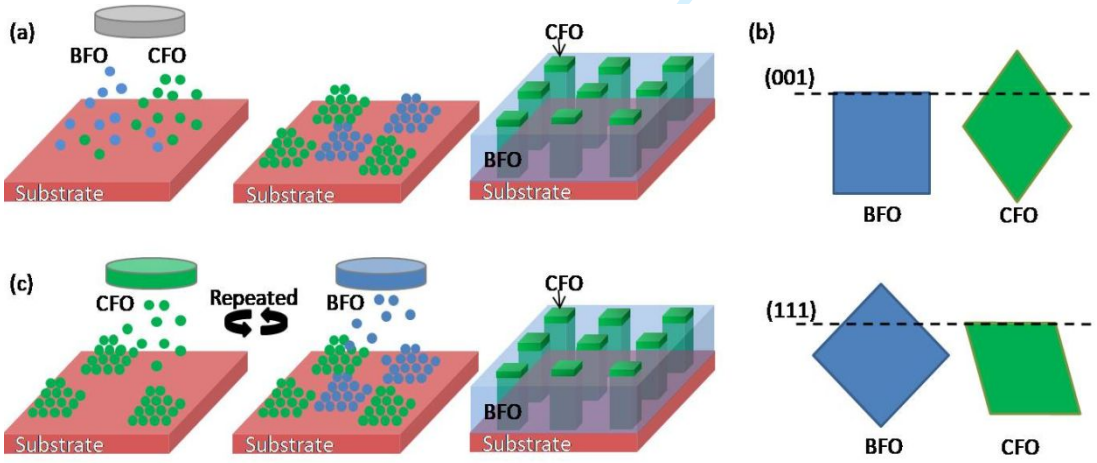

Figure 2. (a) The schematic of the self-assembled BFO-CFO VAN. (b) The illustration of Winterbottom construction resulting from the different on surface energy of BFO and CFO phases.[29] (c) Fabrication of BFO-CFO VAN by PLD method using multiple targets.[5]

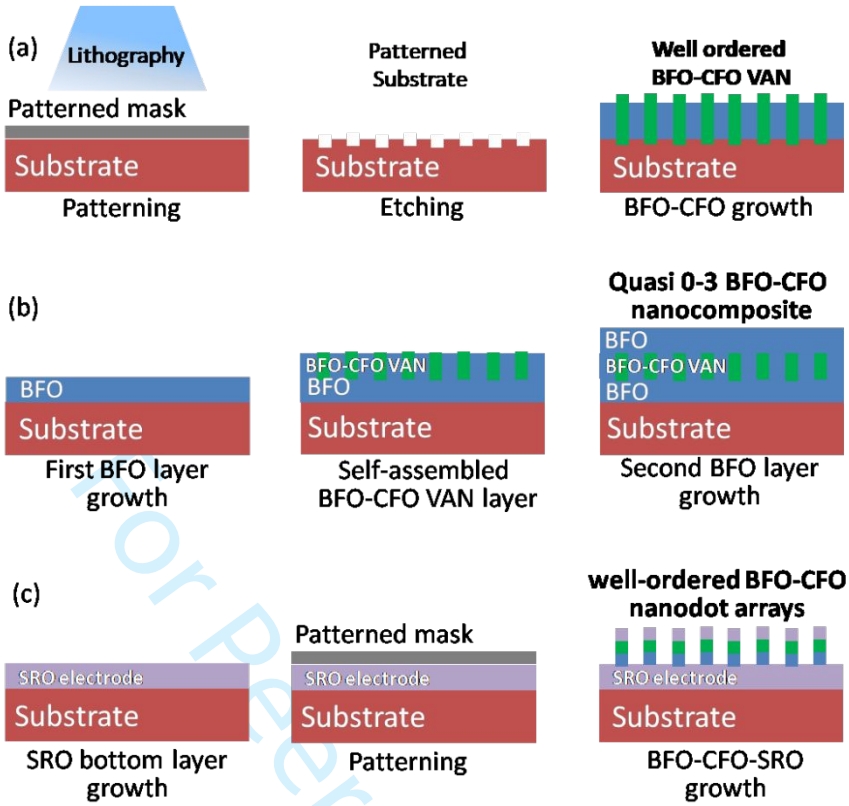

Figure 3. Recent fabrication developments of BFO-CFO VAN by PLD technique. (a) patterning method in order to obtain well-ordered nanopillars.[18] (b) Fabrication of quasi-CFO nanopillars embedded in BFO matrix.[22] (c) Fabrication of well-ordered BFO-CFO nanodot.[20]

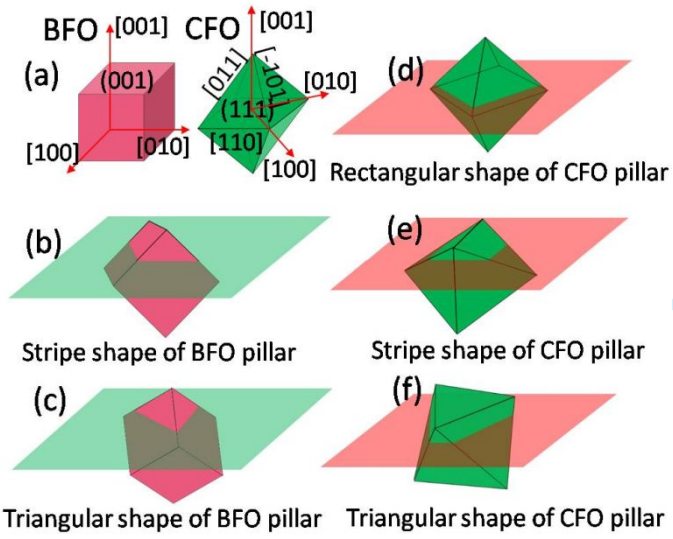

Figure 4. Utilizations of substrate reflect the design of BFO-CFO VAN. Both BFO and CFO could be formed with a specific pattern.

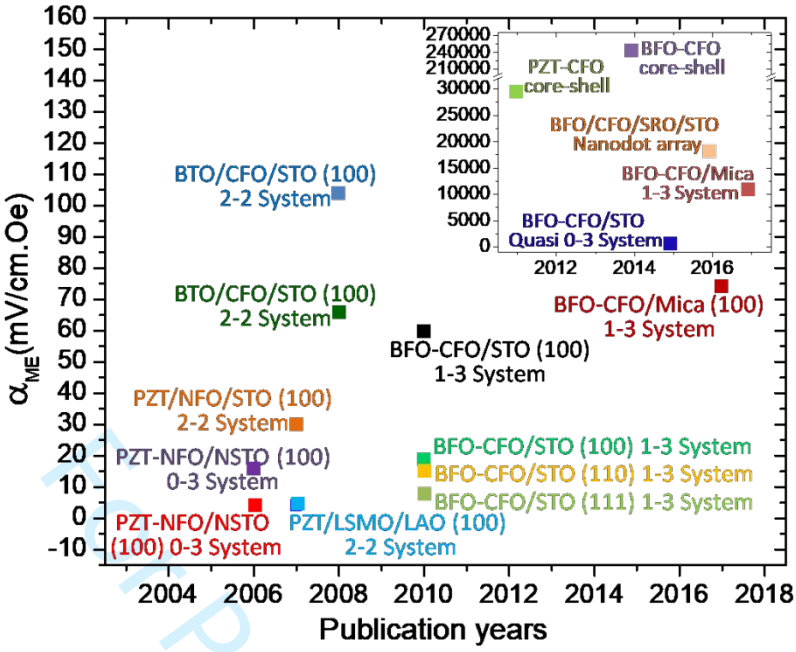

Figure 5. The magnetoelectric coefficient (α_{ME}) from various magnetoelectric composite is determined *via* macroscopic and microscopic (inset Figure) magnetoelectric measurement.

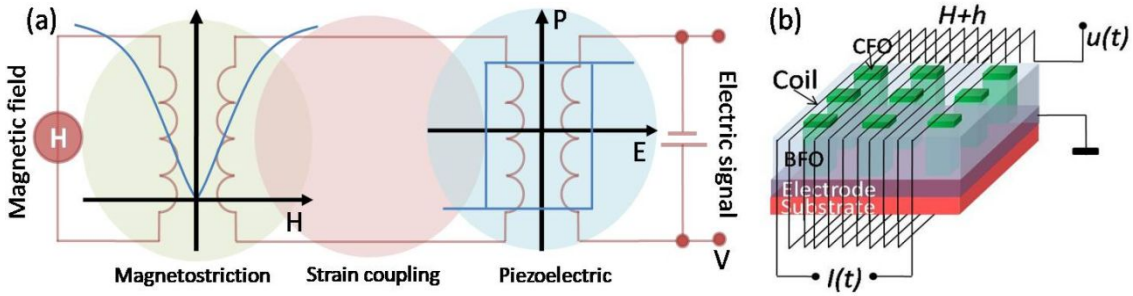

Figure 6. (a) The schematic of strain-mediated magnetoelectric coupling which possible to offers using BFO-CFO VAN system in the magnetic sensor device, adapted from reference.[54] (b) The schematic architecture of the magnetoelectric sensor for DC magnetic fields, adapted from reference.[70]

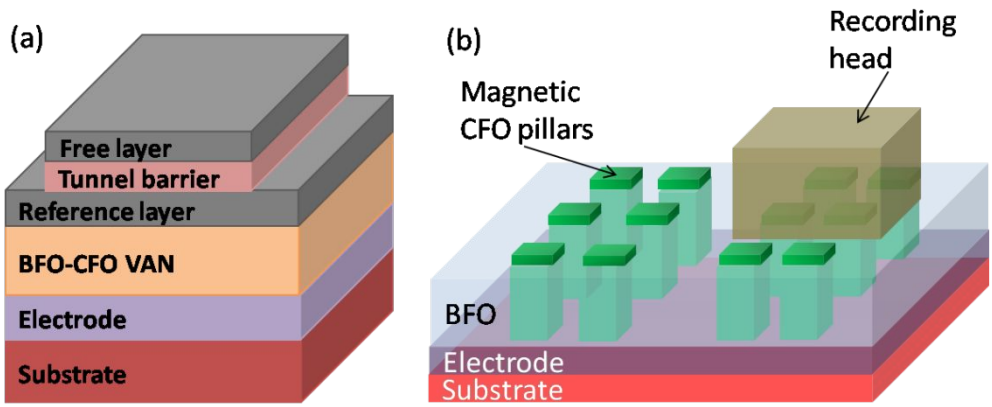

Figure 7. (a) BFO-CFO VAN as the magnetoelectric layer in MTJ device structure.[83] (b) Schematic of bit pattern media utilizing BFO-CFO VAN.

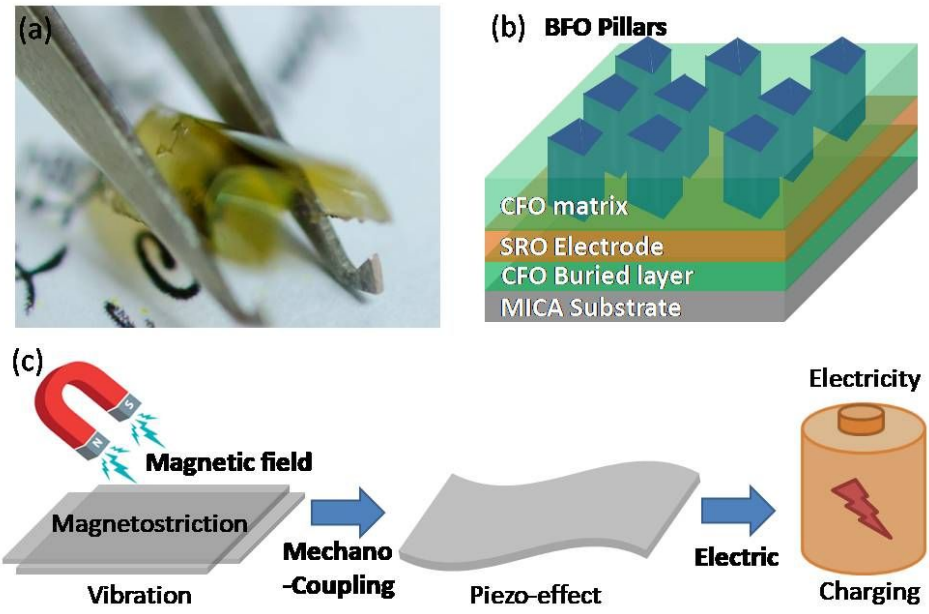

Figure 8. (a) The photograph and (b) the schematic of flexible BFO-CFO/mica, respectively.[9] (c) The schematic scenario of the utilization of flexible BFO-CFO/mica as energy harvesting devices.[6]